
ROBUST FUNCTIONAL PCA FOR DENSITY DATA

A PREPRINT

 **Jeremy Oguamalam***

Institute of Statistics and Mathematical Methods in Economics
TU Wien
Vienna, Austria

 **Peter Filzmoser**

Institute of Statistics and Mathematical Methods in Economics
TU Wien
Vienna, Austria

 **Karel Hron**

Department of Mathematics and Statistics
Palacký University Olomouc
Olomouc, Czechia

 **Alessandra Menafoglio**

Department of Mathematics
Politecnico di Milano
Milan, Italy

 **Una Radojčić**

Institute of Statistics and Mathematical Methods in Economics
TU Wien
Vienna, Austria

January 3, 2025

ABSTRACT

This paper introduces a robust approach to functional principal component analysis (FPCA) for compositional data, particularly density functions. While recent papers have studied density data within the Bayes space framework, there has been limited focus on developing robust methods to effectively handle anomalous observations and large noise. To address this, we extend the Mahalanobis distance concept to Bayes spaces, proposing its regularized version that accounts for the constraints inherent in density data. Based on this extension, we introduce a new method, robust density principal component analysis (RDPCA), for more accurate estimation of functional principal components in the presence of outliers. The method's performance is validated through simulations and real-world applications, showing its ability to improve covariance estimation and principal component analysis compared to traditional methods.

Keywords Relative data · Bayes spaces · Robust principal component analysis · Functional data analysis.

1 Introduction

In the recent decade, functional data analysis (FDA) has grown rapidly (e.g., Ramsay and Silverman (2005)), but there has been less focus on functional distributional data, like density functions. In this context, we do not just understand probability density functions by densities but rather consider a broader class containing relative data that has a functional nature. Examples are age-specific fertility and mortality rates or spectra analysis of different materials. In all these cases, the shape of the underlying curve is of interest, rather than the absolute values taken by the functions.

Densities as random objects need special handling because they are non-negative functions that carry relative information and can be presented with unit integral constraints. This makes compositional data analysis (CoDA) a good framework for densities. By extending CoDA principles to infinite dimensions, densities can be thought of as “infinite-dimensional compositions” and analyzed within a particular Hilbert space called *Bayes spaces* (Egozcue et al., 2006; van den Boogaart et al., 2010).

*The authors gratefully acknowledge support from the Austrian Science Fund (FWF), project number I 5799-N

Functional principal component analysis (FPCA), adapted for Bayes spaces as simplicial functional PCA (SFPCA) (Hron et al., 2016), helps to analyze density data, but its reliance on the sample covariance makes it sensitive to outliers. To address this, a trimmed covariance estimator can be used instead, where center-outwards ordering is used to focus on typical observations. Depth measures provide one possible way to order data that could improve robustness (Fraiman and Muniz (2001); Febrero et al. (2008); López-Pintado and Romo (2009); Arribas-Gil and Romo (2014); Chakraborty and Chaudhuri (2014)). For instance, “spatial depth” has already been useful for data in Bayes spaces Menafoglio et al. (2021). Alternatively, the Mahalanobis distance has been traditionally used for this purpose, and it has been extended to high-dimensional multivariate settings (Secchi et al., 2013), functional settings by, e.g., Galeano et al. (2015); Ghiglietti et al. (2017); Berrendero et al. (2020) for robust covariance estimation, as in the minimum regularized covariance trace (MRCT) estimator (Oguamalam et al., 2024).

The aim of this study is two-fold: first, we extend the concept of regularized Mahalanobis distance for univariate functional data to Bayes spaces, which we will refer to as RDMD. Using the defined notion of Mahalanobis distance, we obtain a robust covariance estimator that further leads to a robust PCA method specifically designed for density data. The resulting procedure is able to handle the density constraints and reduce outlier sensitivity for infinite dimensional compositions.

The rest of the paper is organized as follows: Section 2 discusses the concept of Bayes spaces and SFPCA and showcases potential problems that the outliers in the sample can cause. For an adaptation into the Bayes Hilbert spaces, concepts of data standardization and consequently, the notion of Mahalanobis distance are crucial. In Section 3 we, therefore, propose a way of standardizing (whitening) relative functional data, thus extending and generalizing the notions of truncated- and α -Mahalanobis distance from Galeano et al. (2015) and Berrendero et al. (2020), respectively to Bayes Hilbert spaces. In Section 4, the novel, robust density PCA (RDPCA) method is introduced. Its performance is evaluated in a simulation study and real-data examples in Sections 5 and 6, respectively. Sections 1 and 2 in the supplement provide some additional results, respectively. The final Section 7 concludes with a discussion. Proofs of technical results are given in Supplement Section 3.

2 Preliminaries

In traditional (multivariate) compositional data analysis, the emphasis is on the information found in the relative relationships between variables. This approach led to the development of CoDA based on the Aitchison geometry (Pawlowsky-Glahn et al., 2015). CoDA focuses on positive multivariate observations that are scale invariant, i.e. that can be arbitrarily rescaled equivalence classes of proportional vectors thus form the sample space of compositional data. Along with perturbation and powering operations these concepts form a linear space that operates on the sample space of compositions.

2.1 Bayes space

If we expand the horizon to infinite dimensional compositions, we consider positive functions that are typically represented with unit integral constraint. Intuitively, such compositions can be thought of as density functions. Therefore, statistical concepts designed for unconstrained functional data need to be adapted, as they do not account for this feature, leading to potentially meaningless results when applied to densities (Delicado, 2011; Hron et al., 2016; Menafoglio et al., 2018). Consequently, to work with functional compositions, it is necessary to establish the fundamental concepts of the underlying space structure.

The foundational results were initially presented by Egozcue et al. (2006) and were subsequently extended by van den Boogaart et al. (2010), van den Boogaart et al. (2014) and Talská et al. (2020). The framework for probability density functions is based on a measurable space (Ω, \mathcal{A}) , typically set to $(\mathbb{R}, \mathfrak{B}(\mathbb{R}))$, with $\mathfrak{B}(\mathbb{R})$ as the Borel σ -algebra on \mathbb{R} . Within this space, we consider the set of measures μ that are absolutely continuous with respect to a reference measure λ , here assumed to be the Lebesgue measure with compact support $I = [a, b] \subset \mathbb{R}$. While the authors of van den Boogaart et al. (2014) developed the theory of Bayes space for more general measures λ , in practice, commonly the Lebesgue measure is chosen. Furthermore, usually the measures μ are identified with their respective Radon-Nikodym derivative, density f . For these densities, a notion of equivalence in the Bayes sense for multiples is introduced, i.e. $f =_B g$ if $f = c \cdot g$ for some $c \in \mathbb{R}$. W.l.o.g. within these $(=_B)$ -equivalence classes, we take the element satisfying the unit integral constraint as the representative.

To equip the sample space of these density functions with a structure of a Hilbert space on a given bounded domain, Egozcue et al. (2006) followed the ideas grounding the Aitchison geometry, and extended its operations (\oplus, \odot) (a.k.a.

perturbation and powering), and the inner product $\langle \cdot, \cdot \rangle$ to the infinite-dimensional setting by defining

$$(f \oplus g)(t) =_B f(t)g(t), \quad (\alpha \odot f)(t) =_B (f(t))^\alpha, \quad \langle f, g \rangle_{B^2} =_B \int_I \int_I \log \frac{f(t)}{f(s)} \log \frac{g(t)}{g(s)} dt ds,$$

for densities f, g and $\alpha \in \mathbb{R}$. Endowing the subspace $\mathcal{B}^2(I)$ of positive densities on I with a square-integrable logarithm (van den Boogaart et al., 2014) with this structure yields a separable Hilbert space. In practice, the centered logratio (clr) transformation

$$\text{clr}(f) = \log(f) - \frac{1}{b-a} \int_I (\log(f))(t) dt \quad (1)$$

is used to directly work in a space equipped with a Euclidean structure. Observe that all clr transformed densities satisfy the zero integral constraint.

Denoting $L_0^2(I) \subset L^2(I)$ the set of all square integrable functions on I that additionally integrate to zero, it can be shown that the clr transformation is an isomorphism between $\mathcal{B}^2(I)$ and $L_0^2(I)$, with the corresponding inverse transformation $\text{clr}^{-1}(f) =_B \exp(f)$, for $f \in L_0^2(I)$. The clr transformation (1) enables thus the computation of perturbation, powering, and the inner product of densities through their transformed counterparts in the L^2 space. Let $f, g \in \mathcal{B}^2(I)$ and $\alpha, \beta \in \mathbb{R}$, then

$$\langle f, g \rangle_{B^2} = \langle \text{clr}(f), \text{clr}(g) \rangle_{L^2} \text{ and } \text{clr}((\alpha \odot f) \oplus (\beta \odot g)) = \alpha \cdot \text{clr}(f) + \beta \cdot \text{clr}(g).$$

2.2 Moments of random densities

A Bayes space is a Hilbert space. Therefore, we use the notion of the mean and the covariance in a general Hilbert space structure to specify and inspect the properties of the Bayes mean density $\mu_{B^2, X}$ and Bayes covariance $C_{B^2, X}$ of $X \in \mathcal{B}^2(I)$; see e.g. Kokoszka and Reimherr (2017) for more detail. For a random density $X \in \mathcal{B}^2(I)$, a *Bayes mean density* $\mu_{B^2, X}$ is an object in $\mathcal{B}^2(I)$ satisfying

$$\langle \mu_{B^2, X}, f \rangle_{B^2} = \mathbb{E}(\langle X, f \rangle_{B^2}), \quad (2)$$

for every $f \in \mathcal{B}^2(I)$. Alternatively, the Frechet mean approach used in Petersen et al. (2022) can be used to obtain the same definition. Using the equivalent identity of covariance operators, we define the *Bayes covariance operator* $C_{B^2, X} : \mathcal{B}^2(I) \rightarrow \mathcal{B}^2(I)$ of a random density $X \in \mathcal{B}^2(I)$ as a $\mathcal{B}^2(I)$ operator satisfying

$$\langle C_{B^2, X} f, g \rangle_{B^2} = \mathbb{E}(\langle X \ominus \mu_{B^2, X}, f \rangle_{B^2} \langle X \ominus \mu_{B^2, X}, g \rangle_{B^2}),$$

for every $f, g \in \mathcal{B}^2(I)$. We write

$$C_{B^2, X} = \mathbb{E}((X \ominus \mu_{B^2, X}) \otimes_{B^2} (X \ominus \mu_{B^2, X})),$$

where for $f, g \in \mathcal{B}^2(I)$ the outer product $f \otimes_{B^2} g : \mathcal{B}^2(I) \rightarrow \mathcal{B}^2(I)$ is the linear operator satisfying $(f \otimes_{B^2} g)(h) = \langle g, h \rangle_{B^2} f$, for $h \in \mathcal{B}^2(I)$.

Lemma 2.1 gives the connection between the Bayes mean density $\mu_{B^2, X}$ and covariance $C_{B^2, X}$ and the ‘‘traditional’’ L^2 -mean and the covariance of $\text{clr}(X)$. The proof of Lemma 2.1 can be found in Section (3) of the supplement.

Lemma 2.1 *Let $X \in \mathcal{B}^2(I)$ and $\text{clr}(X) \in L^2(I)$ be its clr transformation. Then the following identities hold:*

- i) $\text{clr}(\mu_{B^2, X}) =_{a.e.} \mathbb{E}(\text{clr}(X))$.
- ii) $\text{clr}(C_{B^2, X} f) =_{a.e.} C_{\text{clr}(X)} \text{clr}(f)$, for every $f \in \mathcal{B}^2(I)$.
- iii) *Let (λ_i, ζ_i) , $i \geq 1$ be the eigenpairs of $C_{B^2, X}$. Then, $(\lambda_i, \text{clr}(\zeta_i) / \int_I \text{clr}(\zeta_i(t)) dt)$, $i \geq 1$ are the eigenpairs of $C_{\text{clr}(X)}$.*

2.3 Simplicial functional PCA

As in the multivariate principal component analysis, functional PCA aims to search for the main modes of variability within a dataset, see e.g. Ramsay and Silverman (2005). More recently, this concept was extended to the Bayes spaces setting in Hron et al. (2016). The authors coined the term *simplicial functional PCA* referring to the simplex, which is

the multivariate counterpart of the Bayes space. More precisely, given a data set $X_1, \dots, X_n \in \mathcal{B}^2(I)$, the problem of finding the first principal function ζ_1 is defined as

$$\max_{\zeta \in \mathcal{B}^2(I)} \frac{1}{n} \sum_{i=1}^n \langle X_i \ominus \hat{\mu}_{B^2, X}, \zeta \rangle_B^2 \quad \text{subject to } \|\zeta\|_B^2 = 1, \quad (3)$$

where $\hat{\mu}_{B^2, X} = \frac{1}{n} \odot \bigoplus_{i=1}^n X_i$ is the sample Bayes-mean. Subsequent components $\{\zeta_i\}_{i \geq 2}$ are then found by the same objective function under the additional orthogonality constraint $\langle \zeta_i, \zeta_j \rangle_{B^2} = 0$ for $j < i$. The principal functions can be found solving the eigenvalue problem

$$\hat{C}_{B^2, X}(\zeta_j) = \lambda_j \odot \zeta_j, \quad j \geq 1 \quad (4)$$

where $\hat{C}_{B^2, X}(Y) = \frac{1}{n} \odot \bigoplus_{i=1}^n \langle X_i \ominus \hat{\mu}_{B^2, X}, Y \rangle_B^2 \odot (X_i \ominus \hat{\mu}_{B^2, X})$ is the sample covariance operator in $\mathcal{B}^2(I)$ and $\lambda_j, j \geq 1$, are its eigenvalues. As discussed in Hron et al. (2016), this problem can be solved in $L^2(I)$ by using the clr transformation; see also Lemma 2.1.

However, as previously emphasized, the eigendecomposition (4) and consequently also the optimization problem (3), are sensitive to the presence of outlying curves in the sample. Therefore, in order to achieve a robust estimation of the functional PCs, the underlying covariance will be based on a sub sample consisting of the most central data points. The centrality of each observation will here be quantified by an adaptation of a regularized functional Mahalanobis distance for densities.

3 Notion of Mahalanobis distance for densities

In recent years, various attempts to extend the concept of multivariate Mahalanobis distance to L^2 spaces have been proposed. The primary challenge in this functional extension is the non-invertibility of the covariance operator in infinite-dimensional cases. For instance, for a fixed p , Galeano et al. (2015) defines the p -truncated Mahalanobis semidistance of $Y \in L^2(I)$ as a Mahalanobis distance of the corresponding optimal rank- p projection; observe that it is indeed only a semidistance, as it lacks identifiability (zero truncated Mahalanobis distance does not necessarily imply a.s. zero process). Additionally, as argued in Berrendero et al. (2020), the partial sums corresponding to the Mahalanobis distance of optimal rank- p projection diverge with p and thus can depend heavily on the choice of p . Ghiglietti et al. (2017) proposed a modification of the approach presented in Galeano et al. (2015) to deal with the convergence issues. Berrendero et al. (2020) introduced the concept of α -Mahalanobis distance, motivated by the Reproducing Kernel Hilbert Space (RKHS) associated with the underlying stochastic process that generates the data.

In a traditional multivariate setting, the Mahalanobis distance $M(\mathbf{x}, \mathbf{y}; \Sigma)$ between two random vectors $\mathbf{x}, \mathbf{y} \in \mathbb{R}^p$ with respect to a regular covariance matrix $\Sigma \in \mathbb{R}^{p \times p}$ can be thought of as a Euclidean distance between the two vectors, previously standardized (whitened) by the common covariance

$$M^2(\mathbf{x}, \mathbf{y}; \Sigma) = (\mathbf{x} - \mathbf{y})' \Sigma^{-1} (\mathbf{x} - \mathbf{y}) = \|\Sigma^{-1/2} \mathbf{x} - \Sigma^{-1/2} \mathbf{y}\|^2.$$

In that manner, the corresponding Mahalanobis norm of a random vector, i.e. the Mahalanobis distance of that random vector from its mean with respect to its covariance, equals the Euclidean norm of that random vector when standardized by its mean and the covariance. That is, $M(\mathbf{x}; \boldsymbol{\mu}, \Sigma) := M(\mathbf{x}, \boldsymbol{\mu}; \Sigma) = \|\mathbf{x}_{\text{st}}\|$, where $\mathbf{x}_{\text{st}} := \Sigma^{-1/2} (\mathbf{x} - \boldsymbol{\mu})$ is a solution to the linear problem $\Sigma^{1/2} \mathbf{x}_{\text{st}} = \mathbf{x} - \boldsymbol{\mu}$ – for more details on whitening of multivariate data see e.g. (Friedman, 1987; Oja et al., 2016; Kessy et al., 2018).

In infinite-dimensional spaces like $L^2(I)$, the covariance is not invertible, implying that this latter linear problem is ill-posed. One of the recent proposals on how to address this problem was given in Oguamalam et al. (2024); Berrendero et al. (2020), using Tikhonov regularization. More specifically, given the regularization parameter $\alpha > 0$, Oguamalam et al. (2024) define the α -standardization of a random function $Y \in L^2(I)$ with mean μ and covariance operator C as a solution to the optimization problem

$$Y_{\text{st}}^\alpha := \arg \min_{Z \in L^2(I)} \left\{ \|C^{1/2} Z - (Y - \mu)\|^2 + \alpha \|Z\|^2 \right\}. \quad (5)$$

Oguamalam et al. (2024) show that the α -Mahalanobis distance is the Euclidean norm of the solution to (5). Regularization in (5) is also known as L^2 -regularization due to penalizing the L^2 -norm of the solution and is perhaps the most widely used penalization form. However, it is often advantageous to consider regularization using a general, non-identity regularization operator $L : L^2(I) \rightarrow L^2(I)$; see e.g. Morigi et al. (2007); Wang (2012).

Here, we extend the optimization problem in (5) to Bayes spaces, allowing for a broader class of regularization operators under general conditions.

3.1 Regularized standardization of density data

Standardization (whitening) is generally defined with respect to the mean and the covariance of the random object being standardized. For the sake of readability, we first discuss the regularized standardization, assuming the mean and the covariance are known.

Let, therefore, $X \in \mathcal{B}^2(I)$, with mean μ_{B^2} and covariance $C_{B^2, X}$ as defined in Section 2. Without loss of generality, assume that X has a constant mean (the neutral element for addition in $\mathcal{B}^2(I)$ is the density of the uniform distribution over I , i.e., a constant function).

Given the closed, densely defined operator $L : \mathcal{B}^2(I) \rightarrow \mathcal{B}^2(I)$ satisfying $\mathcal{N}(C_{B^2, X}^{1/2}) \cap \mathcal{N}(L) = \{0\}$, where $\mathcal{N}(\cdot)$ is the nullspace of the corresponding operator, we define the regularized standardization of $X \in \mathcal{B}^2(I)$ with respect to L as the solution to the optimization problem

$$X_{\text{st}}^{\alpha, L} =_B \arg \min_{Y \in \mathcal{B}^2(I)} \left\{ \|C_{B^2, X}^{1/2} Y \ominus X\|_B^2 + \alpha \|LY\|_B^2 \right\}, \quad (6)$$

where $C_{B^2, X}^{1/2} Y = \bigoplus_{i=1}^{\infty} \lambda_i^{1/2} \langle \zeta_i, Y \rangle_{B^2} \odot \zeta_i$, for (λ_i, ζ_i) , $i \geq 1$ being the i th eigenpair of $C_{B^2, X}$. Observe that $X_{\text{st}}^{\alpha, L}$ is

an approximate solution to $C_{B^2, X}^{1/2} X_{\text{st}}^{\alpha, L} = X$, where α determines that level of approximation. Locker and Prenter (1980) (Theorem 3.1) guarantees the existence and uniqueness of the solution to (6).

For $L = I$ (the identity operator), the optimization problem (6) can be seen as the Bayes space counterpart of the α -standardization in (5). Proposition 3.1 shows the equivalence between (6) in $\mathcal{B}^2(I)$ and (5) in $L^2(I)$ when applied to the clr-transformed density.

Proposition 3.1 *For regularization parameter $\alpha > 0$*

$$X_{\text{st}}^{\alpha, I} =_B \arg \min_{Y \in \mathcal{B}^2(I)} \left\{ \|C_{B^2, X}^{1/2} Y \ominus X\|_B^2 + \alpha \|Y\|_B^2 \right\}$$

if and only if

$$\text{clr}(X_{\text{st}}^{\alpha, I}) = \arg \min_{Z \in L^2(I)} \left\{ \|C_{\text{clr}, X}^{1/2} Z - \text{clr}(X)\|^2 + \alpha \|Z\|^2 \right\},$$

where $C_{B^2, X}$ and $C_{\text{clr}, X}$ are the Bayes space covariance of X and covariance of $\text{clr}(X)$, respectively.

As a corollary of Proposition 3.1, we obtain the explicit solution to (6) for $L = I$.

Corollary 3.1 *Let $X_{\text{st}}^{\alpha, I} =_B \arg \min_{Y \in \mathcal{B}^2(I)} \left\{ \|C_{B^2, X}^{1/2} Y \ominus X\|_B^2 + \alpha \|Y\|_B^2 \right\}$, for regularization parameter $\alpha > 0$. Then*

$$X_{\text{st}}^{\alpha, I} =_B \bigoplus_{i=1}^{\infty} \frac{\lambda_i^{1/2}}{\lambda_i + \alpha} \odot \langle \zeta_i, X \rangle_{B^2} \odot \zeta_i,$$

where (λ_i, ζ_i) is an i -th eigenpair of $C_{B^2, X}$ satisfying $C_{B^2, X} \zeta_i = \lambda_i \odot \zeta_i$, $i \geq 1$.

Choosing the regularization operator. Choosing regularization operators to be orthogonal projectors, as discussed in the work of Morigi et al. (2007), can be particularly advantageous when we have prior knowledge of certain features or structures within the data. A key motivation for using orthogonal projection regularization operators is that it allows us to directly control the components of the solution within the range and null space of L . By projecting onto a subspace that aligns with known properties of the data, we can tailor the regularization to preserve essential characteristics. The following proposition formalizes these insights and provides further motivation for selecting the appropriate regularization strategy by extending the findings of Morigi et al. (2007) (Theorem 2.3) to optimization (6).

Proposition 3.2 *Using the notation and assumptions from Proposition 3.1 let $X_{\text{st}}^{\alpha, L}$ be the unique solution of the minimization problem (6). Consider now the perturbation of the original ill-posed problem $C_{B^2, X}^{1/2} Y = X$ modifying the right hand side as*

$$C_{B^2, X}^{1/2} Y = X \oplus C_{B^2, X}^{1/2} \tilde{X}$$

for some $\tilde{X} \in \mathcal{N}(L)$. Then the unique solution of the associated Tikhonov minimization problem

$$\arg \min_{Y \in \mathcal{B}^2(I)} \left\{ \|C_{B^2, X}^{1/2} Y \ominus (X \oplus C_{B^2, X}^{1/2} \tilde{X})\|_{B^2}^2 + \alpha \|LY\|_{B^2}^2 \right\}$$

is given by $X_{1, \text{st}}^{\alpha, L} = X_{\text{st}}^{\alpha, L} \oplus \tilde{X}$.

If we think of $C_{B^2, X}^{1/2} X_{\text{st}}^{\alpha, L}$ as a regularized approximation of X (see introductory discussion in Section 3.1 and Berrendero et al. (2020)), we get that $C_{B^2, X}^{1/2} X_{1, \text{st}}^{\alpha, L} = C_{B^2, X}^{1/2} X_{\text{st}}^{\alpha, L} \oplus C_{B^2, X}^{1/2} \tilde{X}$, i.e. the perturbed part was recovered exactly. In other words, Proposition 3.2 suggests that the regularization operator should be chosen so that the known features of the desired solution to (6) can be represented using elements in its null space.

For further illustration, we exemplify the result of Proposition 3.2 by considering a regularization operator based on simplicial functional principal components. For this purpose, observe that X admits a Karhunen-Loève representation

$$X = \left(\bigoplus_{i=1}^k \langle X, \zeta_i \rangle_{B^2} \odot \zeta_i \right) \oplus \left(\bigoplus_{i>k} \langle X, \zeta_i \rangle_{B^2} \odot \zeta_i \right),$$

where for $k \geq 0$, such that $\lambda_k > \lambda_{k+1}$, $X_{1:k} := \bigoplus_{i=1}^k \langle X, \zeta_i \rangle_{B^2} \odot \zeta_i$ is the best rank- k approximation of X , and

$X_{(k+1):\infty} := \bigoplus_{i>k} \langle X, \zeta_i \rangle_{B^2} \odot \zeta_i$ the residual. Additionally, it is often argued that the projection of the data onto the first few principal components is an effective way to retain the most significant features of the original dataset (Ramsay and Silverman, 1997; Hron et al., 2016). Consider, therefore, the projection of the data onto the span of the first k eigenfunctions of $C_{B^2, X}$ to be the data feature we would like to preserve. As $C_{B^2, X}^{1/2} X_{1:k} \in \text{span}\{\zeta_1, \dots, \zeta_k\}$, by taking L to be the orthogonal projection onto the complement of $\text{span}\{\zeta_1, \dots, \zeta_k\}$, the regularized approximation $C_{B^2, X}^{1/2} X_{\text{st}}^{\alpha, L}$ of X is of the form $C_{B^2, X}^{1/2} X_{\text{st}}^{\alpha, L} = X_{1:k} \oplus C_{B^2, X}^{1/2} X_{2, \text{st}}^{\alpha, L}$, where $X_{2, \text{st}}^{\alpha, L} \in \text{span}\{\zeta_{k+1}, \zeta_{k+2}, \dots\}$ is the L^2 -regularized standardization of $X_{(k+1):\infty}$.

Thus, denoting $W(k)$ a projection onto the complement of the space spanned by the first $k \geq 0$ eigenfunctions of $C_{B^2, X}$, hereinafter we consider standardization of the form

$$X_{\text{st}, C_{B^2, X}}^{\alpha, k} = \arg \min_{Y \in \mathcal{B}^2(I)} \left\{ \|C_{B^2, X}^{1/2} Y \ominus X\|_{B^2}^2 + \alpha \|W(k)Y\|_{B^2}^2 \right\}, \quad (7)$$

where we add the additional subscript $C_{B^2, X}$ to emphasize that the regularized standardization is performed with respect to $C_{B^2, X}$, and superscript k is used instead of $W(k)$ for simplicity. The following proposition gives the exact form of the solution $X_{\text{st}, C_{B^2, X}}^{\alpha, k}$ and also shows that $\text{clr}(X_{\text{st}, C_{B^2, X}}^{\alpha, k})$ is a solution to the L^2 -equivalent of optimization problem (7).

Proposition 3.3 *Let $X \in \mathcal{B}^2(I)$ be a constant mean random density with Bayes-covariance $C_{B^2, X}$ and let (λ_i, ζ_i) be its i th eigenpair; $C_{B^2, X} \zeta_i = \lambda_i \odot \zeta_i$, $i \geq 1$. For $k \geq 0$, such that $\lambda_k > \lambda_{k+1}$ let $W(k)$ be the projector onto the complement of the space spanned by the first k eigenfunctions ζ_1, \dots, ζ_k of $C_{B^2, X}$. Then there exists a unique solution $X_{\text{st}, C_{B^2, X}}^{\alpha, k}$ of (7). Additionally,*

$$X_{\text{st}, C_{B^2, X}}^{\alpha, k} =_B \arg \min_{Y \in \mathcal{B}^2(I)} \left\{ \|C_{B^2, X}^{1/2} Y \ominus X\|_{\mathcal{B}}^2 + \alpha \|W(k)Y\|_{\mathcal{B}}^2 \right\}$$

if and only if

$$\text{clr}(X_{\text{st}, C_{B^2, X}}^{\alpha, k}) = \arg \min_{Z \in L^2(I)} \left\{ \|C_{\text{clr}, X}^{1/2} Z - \text{clr}(X)\|^2 + \alpha \|V(k)Z\|^2 \right\},$$

where $V(k)$ is the projector of the orthogonal complement onto the space spanned by the first k eigenfunctions of the covariance $C_{\text{clr}, X}$ of $\text{clr}(X)$. In that case,

$$X_{\text{st}, C_{B^2, X}}^{\alpha, k} =_B \sum_{i=1}^k \frac{1}{\lambda_i^{1/2}} \langle X, \zeta_i \rangle_{B^2} \zeta_i \oplus \sum_{i=k+1}^{\infty} \frac{\lambda_i^{1/2}}{\lambda_i + \alpha} \langle X, \zeta_i \rangle_{B^2} \zeta_i.$$

The technical assumption $\lambda_k > \lambda_{k+1}$ ensures well-definiteness of the projector onto the space spanned by the first k eigenfunctions and poses no restriction in practice. Specifically, those PCs having the same variance are considered to be *equally important*, and should then all or none be regularized.

3.2 Regularized Mahalanobis distance for density data

Having introduced the regularized standardization of data in Bayes space, we are ready to define the corresponding regularized Mahalanobis distance for probability density functions.

Definition 3.1 (Regularized Mahalanobis distance between two densities) *Given a constant $\alpha > 0$, and the number of non-regularized components $k \geq 0$, the squared RDMD between $X, Y \in \mathcal{B}^2(I)$, with respect to the covariance operator C is given by*

$$M_{\alpha,k,B^2}^2(X, Y; C) = \|X_{st,C}^{\alpha,k} \ominus Y_{st,C}^{\alpha,k}\|_{B^2}^2,$$

where $X_{st,C}^{\alpha,k}, Y_{st,C}^{\alpha,k}$ are the solutions to

$$\min_{Z \in \mathcal{B}^2(I)} \left\{ \|C^{1/2}Z \ominus X\|_B^2 + \alpha \|W(k)Z\|_B^2 \right\} \quad \text{and} \quad \min_{Z \in \mathcal{B}^2(I)} \left\{ \|C^{1/2}Z \ominus Y\|_B^2 + \alpha \|W(k)Z\|_B^2 \right\},$$

respectively.

The RDMD of random density X is, as in the multivariate setting, defined as the RDMD 3.1 between X and its mean $\mu_{B^2,X}$, with respect to its covariance $C_{B^2,X}$. For the sake of further referencing, the RDMD of $X \in \mathcal{B}^2(I)$ is formally defined as follows.

Definition 3.2 (Regularized Mahalanobis distance for density data) *Given a constant $\alpha > 0$, and the number of non-regularized components $k \geq 0$, the squared RDMD of the random density $X \in \mathcal{B}^2(I)$ with mean $\mu_{B^2,X}$ and covariance $C_{B^2,X}$ is given by*

$$M_{\alpha,k,B^2}^2(X) = M_{\alpha,k,B^2}^2(X, \mu_{B^2,X}; C_{B^2,X}),$$

where $M_{\alpha,k,B^2}^2(X, \mu_{B^2,X}; C_{B^2,X})$ is defined in Definition 3.1. respectively.

The following proposition gives a distribution of the squared RDMD under the assumption of Gaussianity. It also describes how to detect potential outliers by comparing the calculated Mahalanobis distance to an appropriate quantile from the reference distribution.

Proposition 3.4 *Let $X \in \mathcal{B}^2(I)$ be a constant-mean random density such that $\text{clr}(X)$ is a Gaussian random process. Then, for any $\alpha > 0$ and $k \in \mathbb{N}_0$*

$$M_{\alpha,k,B^2}^2(X) \sim \begin{cases} y + \sum_{i=k+1}^{\infty} \frac{\lambda_i^2}{(\lambda_i + \alpha)^2} \eta_i, & \text{for } k \geq 1, \\ \sum_{i=1}^{\infty} \frac{\lambda_i^2}{(\lambda_i + \alpha)^2} \eta_i, & \text{for } k = 0, \end{cases}$$

where $\eta_i \sim \chi^2(1)$, $i \geq 1$ are mutually independent and also independent of $y \sim \chi^2(k)$, and λ_i , $i \geq 1$ is the i th eigenvalue $C_{B^2,X}$.

We conclude this section with a discussion of the connection to the functional MD introduced in Galeano et al. (2015) and Berrendero et al. (2020).

Proposition 3.5 *Let $X \in \mathcal{B}^2(I)$ with w.l.o.g. constant mean $\mu_{B^2,X} \equiv_{B^2} 1$ and $\text{clr}(X) \in L^2(I)$ be the corresponding clr transformation with covariance $C_{\text{clr}(X)} = \sum_{i=1}^{\infty} \lambda_i \xi_i \otimes \xi_i$, where (λ_i, ξ_i) is the i th eigenpair of $C_{\text{clr}(X)}$, such that $\lambda_i > 0$ for $i \leq k$. Let further $M^2(\text{clr}(X); k) = \sum_{i=1}^k \lambda_i^{-1} \langle \text{clr}(X), \xi_i \rangle^2$, and $M_{\alpha}^2(\text{clr}(X)) = \sum_{i=1}^{\infty} \frac{\lambda_i}{(\lambda_i + \alpha)^2} \langle \text{clr}(X), \xi_i \rangle^2$ be the k -truncated Mahalanobis distance (Galeano et al., 2015, Definition 2.1) and α -Mahalanobis distance (Berrendero et al., 2020, Definition 1), respectively. The following identities then hold:*

- i) $M_{\alpha,0,B^2}^2(X) = M_{\alpha}^2(\text{clr}(X))$,
- ii) $\lim_{\alpha \rightarrow \infty} M_{\alpha,k,B^2}^2(X) = M^2(\text{clr}(X); k)$.

Proposition 3.5 shows that functional MD introduced by Galeano et al. (2015); Berrendero et al. (2020) can be regarded as extreme cases of the RDMD from Definition 3.2.

4 Robust density PCA (RDPCA)

4.1 Robust Bayes covariance estimation

Given the data sample X_1, \dots, X_n and a subset $H \subseteq \{1, \dots, n\}$, $|H| = h \in [n/2, n]$ we define the trimmed Bayes mean and covariance estimators calculated using an H -subset of the data as

$$\hat{\mu}_{B^2, H} = \frac{1}{h} \odot \bigoplus_{i \in H} X_i, \quad \hat{C}_{B^2, H, c_H} = c_H \frac{1}{h} \odot \bigoplus_{i \in H} (X_i \ominus \hat{\mu}_{B^2, H}) \otimes_{B^2} (X_i \ominus \hat{\mu}_{B^2, H}).$$

The constant c_H is a scaling factor to adjust for trimming and is determined under the assumption of Gaussianity. For that purpose, we present the next corollary which is an analogue of Proposition 3.4 on the sample level.

Corollary 4.1 *Let $X \in \mathcal{B}^2(I)$ be a random density such that $\text{clr}(X) \in L^2(I)$ is a Gaussian random process, and let $\hat{C}_{B^2, X}$ and $\hat{\mu}_{B^2, X}$ be strongly consistent estimators of the covariance operator $C_{B^2, X}$ and the constant mean $\mu_{B^2, X} \equiv_{B^2} 1$, respectively. Then, for $\alpha > 0$ and $k \in \mathbb{N}_0$, such that $\lambda_k > \lambda_{k+1}$, $M_{\alpha, k, B^2}^2(X, \hat{\mu}_{B^2, X}; \hat{C}_{B^2, X})$ converges in distribution to*

$$M_{\alpha, k, B^2}^2(X) \sim \begin{cases} y + \sum_{i=k+1}^{\infty} \frac{\lambda_i^2}{(\lambda_i + \alpha)^2} \eta_i, & \text{for } k \geq 1, \\ \sum_{i=1}^{\infty} \frac{\lambda_i^2}{(\lambda_i + \alpha)^2} \eta_i, & \text{for } k = 0, \end{cases}$$

where $\eta_i \sim \chi^2(1)$, $i \geq 1$ are mutually independent and also independent of $y \sim \chi^2(k)$, and λ_i , $i \geq 1$ is the i th eigenpair of $C_{B^2, X}$.

For more details on the necessity of scaling the trimmed covariance, see, e.g., Boudt et al. (2020); Oguamalam et al. (2024).

Using the notion of RDMD as a centrality measure, we choose the trimming subset H_0 as a solution to

$$H_0 = \arg \min_{\{H \subset \{1, \dots, n\}; |H|=h\}} \frac{1}{h} \sum_{i \in H} M_{\alpha, k, B^2}^2(X_i, \mu_{B^2, X}; C_{B^2, X}), \quad (8)$$

where $\alpha > 0$ and $k \in \mathbb{N}_0$ are a priori chosen regularization parameters.

Since the true mean and covariance operator are unknown, we replace them in (8) with the current robust estimates. This approach leads to an implicit equation for obtaining the optimal subset:

$$H_0 = \arg \min_{\{H \subset \{1, \dots, n\}; |H|=h\}} \frac{1}{h} \sum_{i \in H} M_{\alpha, k, B^2}^2(X_i, \hat{\mu}_{B^2, H_0}; \hat{C}_{B^2, H_0, c_{H_0}}). \quad (9)$$

Oguamalam et al. (2024) (Lemma 3.1) guarantees that the implicit equation (9) has a solution.

Finally, Corollary 4.1 implies that c_{H_0} can be estimated by matching the sample median of $\{M_{\alpha, k, B^2}^2(X_i, \hat{\mu}_{B^2, H_0}; \hat{C}_{B^2, H_0, c_{H_0}}), i = 1, \dots, n\}$ with the estimate of the median of the corresponding limiting distribution given in Corollary 4.1, where the eigenvalues λ_i , $i \geq 1$ of $C_{B^2, X}$ are again replaced by their robust estimates;

$$c_{H_0} = \text{med} \left\{ M_{\alpha, k, B^2}^2(X_i, \hat{\mu}_{B^2, H_0}; \hat{C}_{B^2, H_0, c_{H_0}}), i = 1, \dots, n \right\} / \text{med} \left\{ y + \sum_{i=k+1}^{\infty} \frac{\lambda_i^2}{(\lambda_i + \alpha)^2} \eta_i \right\},$$

where $\eta_i \sim \chi^2(1)$, $i \geq 1$, are mutually independent and are independent of $y \sim \chi^2(k)$ for $k \geq 1$.

4.2 Algorithm

We solve (9) iteratively, replacing the RDMD in the j th iteration with its estimate using the $(j-1)$ st optimal subset:

$$H_j = \arg \min_{\{H \subset \{1, \dots, n\}; |H|=h\}} \frac{1}{h} \sum_{i \in H} \hat{M}_{\alpha, k, B^2}^2(X_i, \hat{\mu}_{B^2, H_{j-1}}; \hat{C}_{B^2, H_{j-1}, c_{H_{j-1}}}), \quad (10)$$

where $\hat{\mu}_{B^2, H_{j-1}}$ and $\hat{C}_{B^2, H_{j-1}, c_{H_{j-1}}}$ are the trimmed sample mean and covariance operator based on the subset H_{j-1} , respectively. Thus, in the j th step of the procedure, we identify h observations with the smallest regularized Mahalanobis distances to the robust mean estimate $\hat{\mu}_{B^2, H_{j-1}}$, w.r.t. the current robust covariance estimate $\hat{C}_{B^2, H_{j-1}, c_{H_{j-1}}}$.

In practice, it is important to note that we do not observe smooth density functions directly. Instead, we either see discrete realizations of each underlying functional observation or the data sets used to estimate these densities. A common approach for density estimation is kernel-based density estimation, where densities are estimated on an arbitrarily dense, regular grid. Let therefore $X_i(t) : t \in \{t_1, \dots, t_p\}$, $i = 1, \dots, n$, be a discretely observed sample.

Since we observe only a discrete set of functional values for each function X_i , $i = 1, \dots, n$, both X_i and $\hat{\mu}_{B^2, H_{j-1}}$ are represented as large vectors. The covariance $\hat{C}_{B^2, H_{j-1}, c_{H_{j-1}}}$ is similarly replaced with a matrix of sample estimates of the pointwise covariances at observed points. If p is chosen large enough, however, functional inner products used in estimating the RDMD can be well approximated by integral sums; see e.g. Ostebee and Zorn (2002) for more detail on integral approximations. Once robust pointwise estimates of the covariance (and PCs) are obtained, interpolation can be applied to extend these estimates over the entire domain, though that lies beyond the scope of this paper.

The strategy for finding the solution to (10), and consequentially robust principal components, results in a concentration-step-type algorithm (Rousseeuw and Driessen, 1999) and is presented in Algorithm 1, where for simplicity of notation we assume $p \geq n$ and $k \geq 1$.

Algorithm 1: RDPCA

Input: sample $X_1, \dots, X_n \in \mathcal{B}^2$ observed at p time points t_1, \dots, t_p , an initial subset $H_1 \subset \{1, \dots, n\}$, $|H_1| = h$, regularization parameter $\alpha > 0$, projection dimension $k \leq n$, and the tolerance level $\varepsilon_k > 0$;

```

1  $Y_i \leftarrow \text{clr}(X_i)$ ,  $i = 1, \dots, n$ ; do
2    $H_0 \leftarrow H_1$ ;
3   Sample mean:  $\bar{Y}_{H_0} \leftarrow \frac{1}{h} \sum_{i \in H_0} Y_i$ ;
4   Non-scaled covariance:  $\hat{C}_{\text{clr}, H_0} \leftarrow \frac{1}{h} \sum_{i \in H_0} (Y_i - \bar{Y}_{H_0}) \otimes (Y_i - \bar{Y}_{H_0})$ ;
5   Calculate spectral decomposition  $\hat{C}_{\text{clr}, H_0} = \sum_{i \geq 1} \hat{\lambda}_{i, H_0} \hat{\xi}_{i, H_0} \otimes \hat{\xi}_{i, H_0}$ ;
6   Set initial scaling parameter  $c_{1, H_0} \leftarrow 1$ ;
7   do
8      $c_{0, H_0} \leftarrow c_{1, H_0}$ ;
9     Set  $\hat{V}(k) \leftarrow I - \sum_{i=1}^k \hat{\xi}_{i, H_0} \otimes \hat{\xi}_{i, H_0}$ ;
10    Standardization:  $Y_{i, \text{st}, H_0}^{\alpha, k} = \left( \hat{C}_{\text{clr}, H_0} + \alpha / c_{0, H_0} \hat{V}(k) \right)^{-1} \hat{C}_{\text{clr}, H_0}^{1/2} (Y_i - \bar{Y}_{H_0})$ ;
11     $d_{i, H_0, c_0}^2 \leftarrow \|Y_{i, \text{st}, H_0}^{\alpha, k}\|^2$ ;
12    Generate  $\eta_{k+1}, \dots, \eta_n \sim \chi^2(1)$ ,  $y \sim \chi^2(k)$ ;
13     $c_{1, H_0} \leftarrow \frac{\text{med} \{d_{i, H_0, c_0}^2 : i = 1, \dots, n\}}{\text{med} \left\{ y + \sum_{i=k+1}^{\infty} \frac{\lambda_i^2}{(\lambda_i + \alpha)^2} \eta_i \right\}}$ ;
14    while  $(c_{1, H_0} - c_{0, H_0})^2 \geq \varepsilon_k$ ;
15    Order  $d_{(i_1, H_0, c_1)}^2 \leq \dots \leq d_{(i_n, H_0, c_1)}^2$ ;
16    Set  $H_1 \leftarrow \{i_1, \dots, i_h\}$ ;
17 while  $H_0 \neq H_1$ ;
18 Solve symmetric eigenproblem  $h^{-1} c_{1, H_1} \hat{C}_{\text{clr}, H_1}(\xi_j) = \lambda_j \xi_j$ ;
19 Set  $\hat{\xi}_{j, H_{\text{opt}}} \leftarrow \xi_j$ ,  $\hat{c}_{j, H_{\text{opt}}} = \text{clr}^{-1}(\xi_j)$  and  $\hat{\lambda}_{j, H_{\text{opt}}} \leftarrow \lambda_j$ ;
Output: Optimal subset  $H_{\text{opt}} := H_1$ , scaling factor  $c_{H_0}$ , squared robust RDMD  $(c_{1, H_0}^{-1} d_{(1, H_0, c_1)}^2, \dots, c_{1, H_0}^{-1} d_{(n, H_0, c_1)}^2)$ , robust
eigenvalues  $\{\hat{\lambda}_{j, H_{\text{opt}}}\}_{j \geq 1}$  and corresponding robust FPCs  $\{\hat{\xi}_{j, H_{\text{opt}}}\}_{j \geq 1}$ ,  $\{\hat{\xi}_{j, H_{\text{opt}}}\}_{j \geq 1}$  in Bayes and clr space,
respectively.

```

Alternatively, in the case where the discretely observed data has been converted into a functional form, in particular via finite basis smoothing, an adaptation of Algorithm 1 involves calculations to be based on the matrix of the coefficients of the basis expansion, and can be done as described in Oguamalam et al. (2024).

Selecting the regularization parameters The regularized Mahalanobis distance depends on the tuning parameters $\alpha > 0$ and $k \in \mathbb{N}_0$. The choice of α balances the smoothness of the regularized data with how well it fits the observed data. If α is too large, over-regularization will result in poor fit, with large residuals $\|\hat{C}_{B^2, H_{\text{opt}}}^{1/2} (X_{i, \text{st}, \hat{C}_{B^2, H_{\text{opt}}}}^{\alpha, k}) \ominus X_i\|_{B^2}^2$, $i = 1, \dots, n$. Conversely, if α is too small, the solution will overfit data errors, leading to large values of $\|\hat{W}(k) X_{i, \text{st}, \hat{C}_{B^2, H_{\text{opt}}}}^{\alpha, k}\|^2$.

To determine α , we adapt the approach from Oguamalam et al. (2024), iteratively adjusting α so that the Bayes covariance of the standardized data has eigenvalues close to zero (for the latter part of the spectrum) or some fixed constant (for the signal part), thus maximizing the signal-to-noise ratio.

On the other hand, we can think of k as a certain over-smoothing parameter that prevents important signal features from being over-smoothed. Hron et al. (2016) argues how for densities from the k_0 -exponential family (with k_0 parameters), the number of principal components belonging to strictly positive eigenvalues is precisely k_0 . E.g., for the Gaussian family with the known mean $k_0 = 1$; see Hron et al. (2016) for more details. Therefore, in the Sections 5 and 6 we fix $k = 1$.

5 Simulations

In the following two sections, we investigate the robustness of Algorithm 1 against data sets where a fixed proportion c of the data has been replaced by outliers and compare it to the non-robust SFPCA method.

5.1 Simulation 1

In the first simulation, in each of 100 repetitions, we consider a data set of size $n = 200$ consisting of $n - \lfloor cn \rfloor$ regular- and $\lfloor cn \rfloor$ contaminated curves. Each curve is estimated using kernel density estimation (KDE) on a generated sample and evaluated at an equidistant grid of $p = 50$ time points. The construction of a regular/outlying sample is as follow:

$$X_{\text{reg}} = \text{KDE}(Y_1, \dots, Y_N), X_{\text{out}} = \text{KDE}(Y_1, \dots, Y_N, \tilde{Y}_1, \dots, \tilde{Y}_{\lfloor 0.1N \rfloor})$$

where $Y_i \sim N(0, 1)$, $\tilde{Y}_i \sim U([q_1; q_2] \cup [-q_2; -q_1])$, $N = 250$ and q_1, q_2 being the 0.1% and 0.5% quantile of the standard normal distribution, respectively. KDE was calculated using the R-package `kde1d` (Nagler, 2024).

By the construction of these densities, a fixed proportion c of the data is contaminated within the tails of the distribution. Figure 1 presents an example of this model, displaying both the densities and their transformed counterparts, for a contamination rate of $c = 0.2$. In the supplement, we extend this simulation with two additional models, where the densities are constructed in a similar fashion for different distributions of Y_i and \tilde{Y}_i .

To measure the performance of RDPCA, we consider two statistics: the integrated square error (ISE), approximating the norm of the difference between estimates of the true and sub-sampled covariances, and the mean cosine between the first five pairs of eigenfunctions based on the same estimates. For more details, see Supplement Section 1.

During the analysis, we consider contamination rates $c \in \{0, 0.05, 0.1, 0.2\}$, automatically select the regularization parameter α according to the procedure discussed in Section 4.2. Furthermore, we fix $h = \lceil 0.75n \rceil$ and $k = 1$. The results w.r.t. contamination rate c are shown in Figure 2, where the mean value over 100 repetitions \pm one standard error are depicted. Both the ISE and the mean cosine suggest that RDPCA significantly outperforms SFPCA in the presence of outliers.

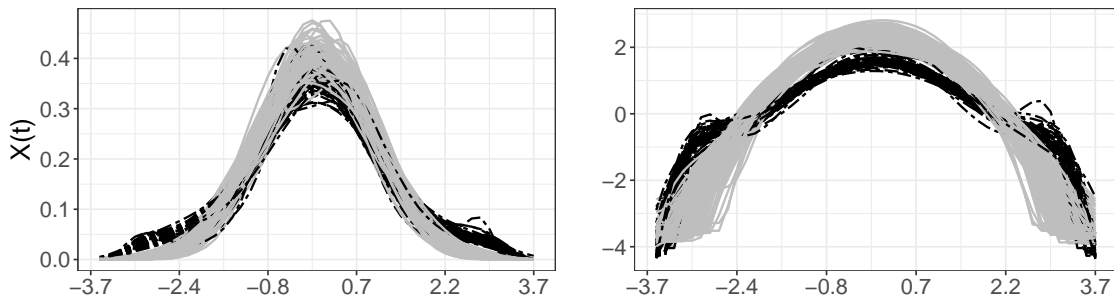


Figure 1: Visualization of density functions (left) and clr transformed counterparts (right). Solid curves represent the main processes, while the dashed ones indicate the outliers.

In Figure 3, the robust correlation function nicely aligns with the correlation function based on a Monte Carlo estimate of the true underlying model. On the contrary, the non-robust correlation reveals significantly different structure. Below, in Figure 4 we compare the squared RDMD based on these two sample estimates and the squared robust α -Mahalanobis (Berrendero et al., 2020) distance, ignoring the compositional structure of the densities. The dashed lines indicate the

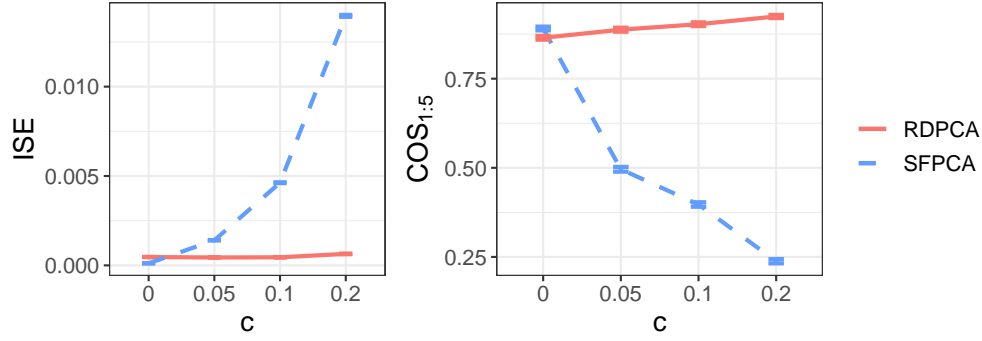


Figure 2: Integrated square error (left) and mean cosine (right) between first five pairs of estimated and true eigenfunctions. Displayed are the mean \pm one standard error of each measurement over all iterations at each level of the corresponding parameter configuration. All measurements are calculated based on the covariance estimated by RDPCA (solid) and SFPCA (dashed) and respectively compared with the estimated true covariance.

95% quantile of the limiting distribution of these distances assuming Gaussianity; see Corollary 4.1. These values are estimated by Monte Carlo simulation. Then, a density is considered outlying if its squared Mahalanobis distance exceeds this cutoff. The circles represent the true regular observations, whereas the triangles correspond to the outliers. According to the cutoff values, only RDPCA can determine outliers in a meaningful way. In the supplement, we added some additional results related to this comparison.

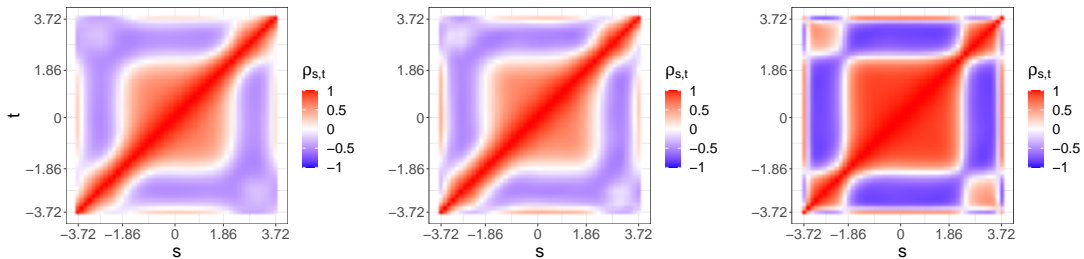


Figure 3: True (left), RDPCA with $\alpha = 0.48$ (middle), and SFPCA (right) correlation function, for the example shown in Figure 1.

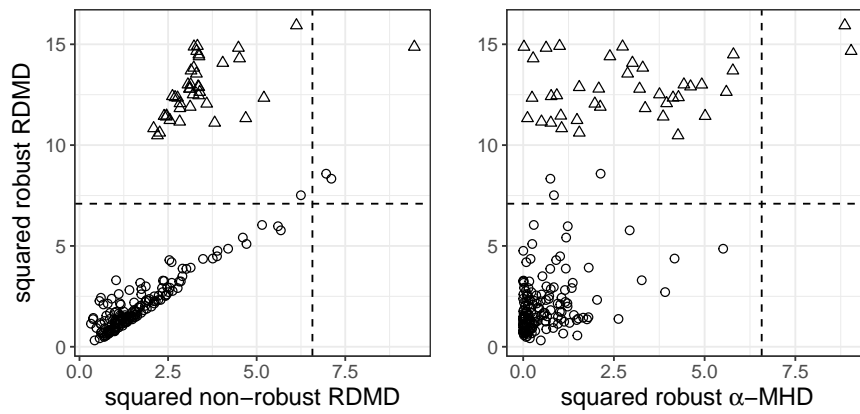


Figure 4: Distance-distance plot of squared robust vs. non-robust RDMD (left) and robust α -Mahalanobis (Berrendero et al., 2020) (right) distances for example of Figure 1. The regularization parameter is $\alpha = 0.48$. Dashed lines indicate the corresponding cutoff values, under Gaussianity. Circles and triangles correspond to true regular and outlying observations, respectively.

5.2 Simulation 2

In the second simulation, we generate data sets of size $n = 200$ according to

$$\begin{aligned}\text{clr}(X_{\text{reg}}(t)) &= s_1\xi_1 + s_2\xi_2 + s_3\xi_3 + s_4\xi_4, \\ \text{clr}(X_{\text{out}}(t)) &= s_1\xi_1 + s_2\xi_2 + s_3\xi_3 + s_4\xi_4 + s_5\xi_5,\end{aligned}$$

where $\xi_1 = \sqrt{2}\sin(2\pi t)$, $\xi_2 = \sqrt{2}\cos(2\pi t)$, $\xi_3 = \sqrt{2}\sin(4\pi t)$, $\xi_4 = \sqrt{2}\cos(4\pi t)$ are the eigenfunctions of the covariance operator of the clr transformed densities. The coefficients s_1, s_2, s_3, s_4 are the associated scores, following a specified distribution. Additionally, the expansion of the outliers is extended by a linear trend, $\xi_5 \propto t$ such that $\int_I \xi_5(t)dt = 0$.

We either consider scores that independently follow a normal distribution, i.e. $s_i \sim N(0, \lambda_i)$ or jointly a multivariate t-distribution, i.e. $(s_1, s_2, s_3, s_4) \sim t_5(\mathbf{0}, \text{diag}(\lambda_1, \lambda_2, \lambda_3, \lambda_4))$ and $(s_1, s_2, s_3, s_4, s_5) \sim t_5(\mathbf{0}, \text{diag}(\lambda_1, \lambda_2, \lambda_3, \lambda_4, \lambda_5))$. In both cases we set $(\lambda_1, \lambda_2, \lambda_3, \lambda_4, \lambda_5) = (2, 1, 1/2, 1/4, 4)$. The resulting process is then evaluated at an equidistant grid of $p = 100$ time points. Figure 5 shows an example of the proposed model. For more details on the extension and the analysis of a second model, we refer to the supplement.

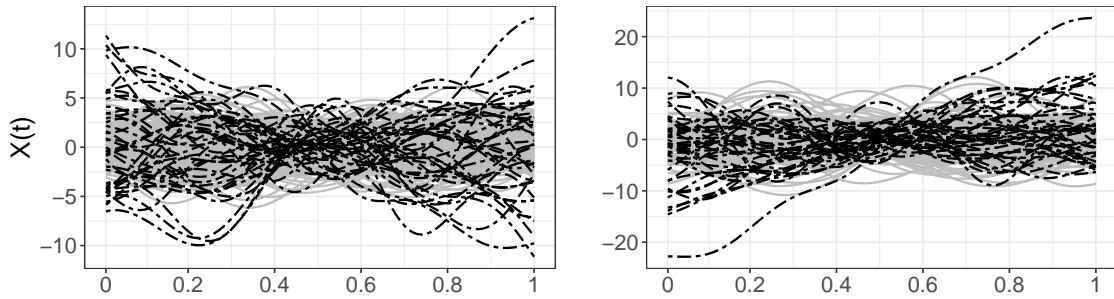


Figure 5: Visualization of curves for normal (left) and multivariate t-distributed (right) scores. Solid curves represent the main processes, dashed ones indicate outliers.

Each setting is again replicated 100 times for $c = \{0, 0.05, 0.1, 0.2\}$ and analyzed using automatically selected α , $h = \lceil 0.75n \rceil$, $k = 1$. The accuracy of RDPCA is evaluated by the ISE of the difference between the estimated and the true covariance, as well as the mean cosine between the first four pairs of eigenfunctions based on the estimated and the true covariance. The corresponding results are shown in Figure 6.

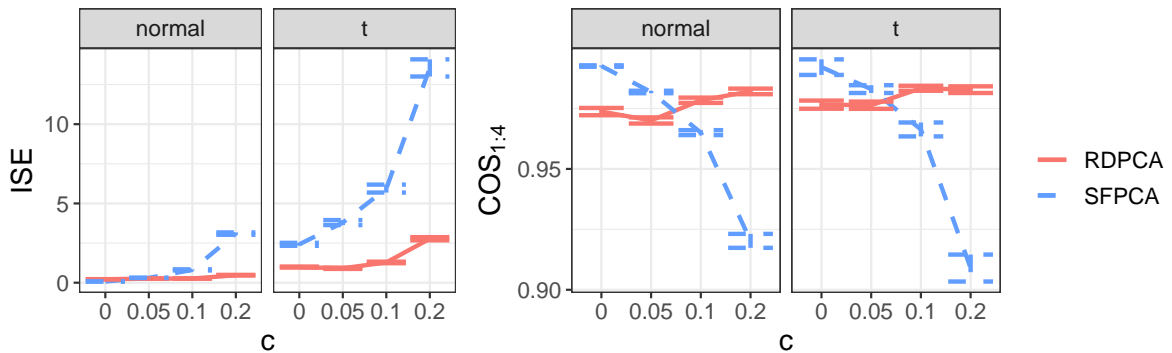


Figure 6: Integrated square error (left) and cosine between first four pairs of estimated and true eigenfunctions (right). Displayed are the mean \pm one standard error of each measurement over all iterations at each level of the corresponding parameter configuration. All measurements are calculated based on the covariance estimated by RDPCA (solid) and SFPCA (dashed) and respectively compared with a true covariance function. The notation “normal” and “t” refer to the distribution of the scores in the underlying model as described at the beginning of this section.

In the final analysis, we contrast the estimated ratio of explained variance between robust and non-robust approaches to the true proportions. The results presented in Figure 7 show that the robust methodology is able to accurately estimate the true ratios.

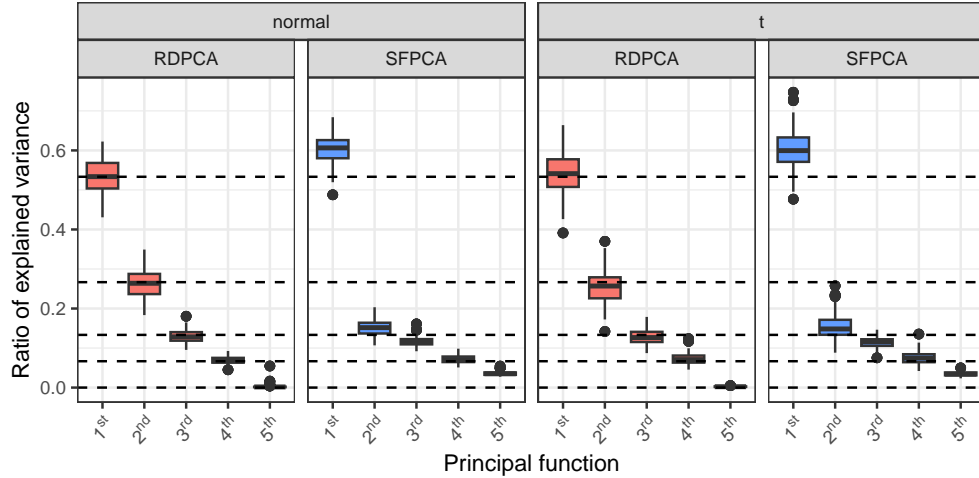


Figure 7: Estimated ratio of explained variance for the first five principal functions over different score distributions at $c = 0.2$. The dashed reference lines depict the true proportion. The notation “normal” and “t” refer to the distribution of the scores in the underlying model as described at the beginning of this section.

6 Real-data example

6.1 EPXMA spectra

The considered dataset consists of electron probe X-ray microanalysis (EPXMA) spectra of various glass vessel types. This type of analysis is commonly used to determine the chemical composition of glasses by measuring X-rays at different wavelength emitted from a sample after being hit by a beam of electrons. The resulting intensities are inherently relative. Furthermore, due to the mutual influence chemical elements have on each other during this process, it is reasonable to view EPXMA spectra as relative functional data.

The dataset contains 180 such observations divided into four distinct groups corresponding to different glass vessel types. The largest group, referred to as “sodic”, comprises 145 spectra. The remaining groups, designated as “potassic”, “potasso-calcic”, and “calcic” are represented by 15, 10, and 10 spectra, respectively. It is important to note that the latter 38 spectra within the sodic group were acquired under varying experimental conditions. Each observation is characterized by measurements across 1920 wavelengths. For the purposes of this analysis, we focus on the initial 750 wavelengths as these encompass the primary variability observed in the data; for more details see Lemberge et al. (2000). This results in $n = 180$, $p = 750$.

The left plot of Figure 8 shows the trajectories of all clr transformed observations colored according to their respective glass vessel type. For the analysis, we consider the first 107 observations from the sodic group as regular observations. We select $\alpha = 0.09$ as in Section 19. Additionally, we have $h = \lceil 0.5n \rceil$ and $k = 1$.

The right plot of Figure 8 displays the squared robust versus the non-robust RDMD. The non-robust approach detects virtually no outlying observations, while the robust procedure can clearly differentiate between the majority of “sodic” and the remaining observations.

Consequently, the structure of the covariance or correlation function can also be significantly influenced in the presence of outlying curves. This is showcased in Figure 9 where robust and non-robust correlations are compared. Between wavelength 100 to 250 and around 400, the outliers exhibit a different structure. Especially at these parts of the domain, the non-robust correlation shows its bias towards the outlying curves.

6.2 Fertility data

The second data set considered in this study focuses on age-specific fertility rates (ASFR) across different countries. ASFR represents the number of women giving birth per 1,000 within specific age groups, providing a detailed view of how fertility changes with age. The resulting curves are analyzed as density data because we are interested in the underlying distribution across the different age groups rather than the magnitude of it. We examine data from the Human Fertility Database, freely available at

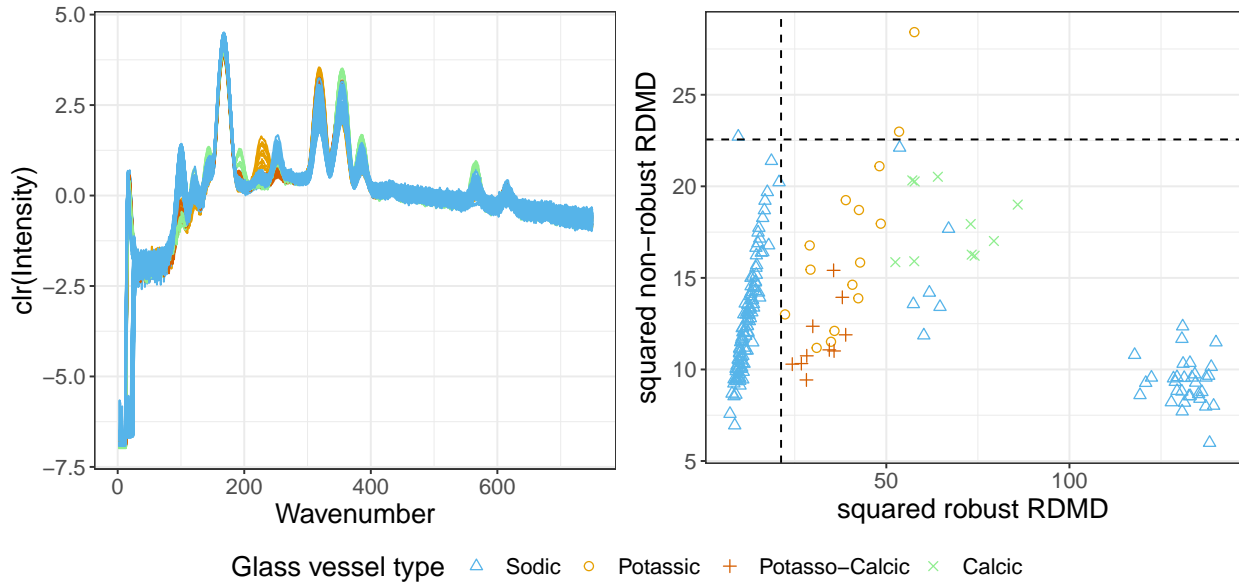


Figure 8: Left: clr transformed spectra colored according to glass vessel type. Right: Distance-distance plot of the squared robust vs. non-robust RDMD. Dashed lines indicate the theoretical cutoff values under Gaussianity.

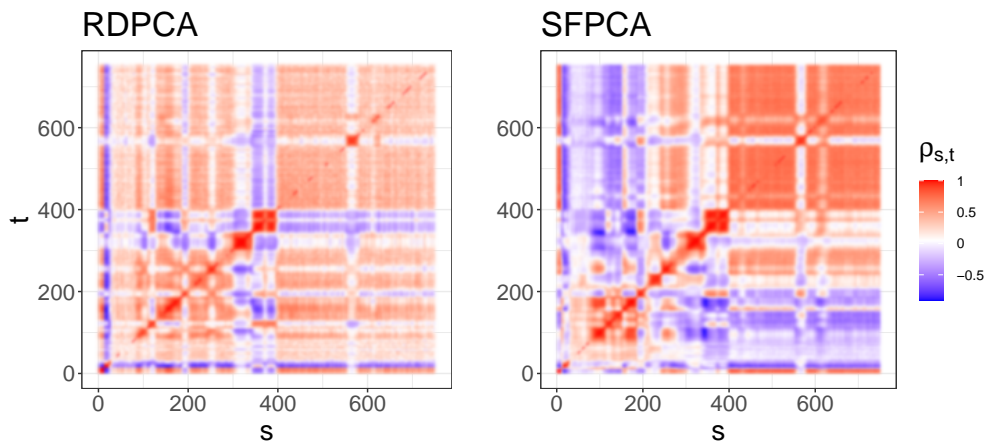


Figure 9: Correlation function of EPXMA data based on RDPCA and SFPCA.

<https://www.humanfertility.org/Home/Index>, focusing on the years 1956, 1990, and 2019, to gain insight in the evolution fertility dynamics.

In the left column of Figure 10 we display the fertility densities. Outlying countries according to Algorithm 1 are represented by dashed curves. During the early stages of this period, peak fertility was primarily achieved by young women in their early 20s. Large families were common, reflected in a rather slow decrease in the majority of the fertility curves. During the following decades, mostly influenced by the introduction of reliable contraceptives and a change in the mindset about life quality, later first-pregnancies became more and more common. Throughout Europe, this phenomenon started earlier in the West than in the East, as can be seen by the fertility curves corresponding to the year 1990. Since then, the peak fertility has steadily increased and sits now at around 30 years. For more details we refer to the insightful article by Beaujouan (2020) and references therein.

While the variability in the Bayes space seems to be present within the peaks, the upper row of Figure 10 shows that the main variability within the clr space is significantly higher in the tails of the distribution; see also (Hron et al., 2016).

In Figure 11 the first two principal functions are displayed. In the brackets, we included the corresponding percentage of explained variance. As assessed before, for each year, the first component mainly captures the variability in the

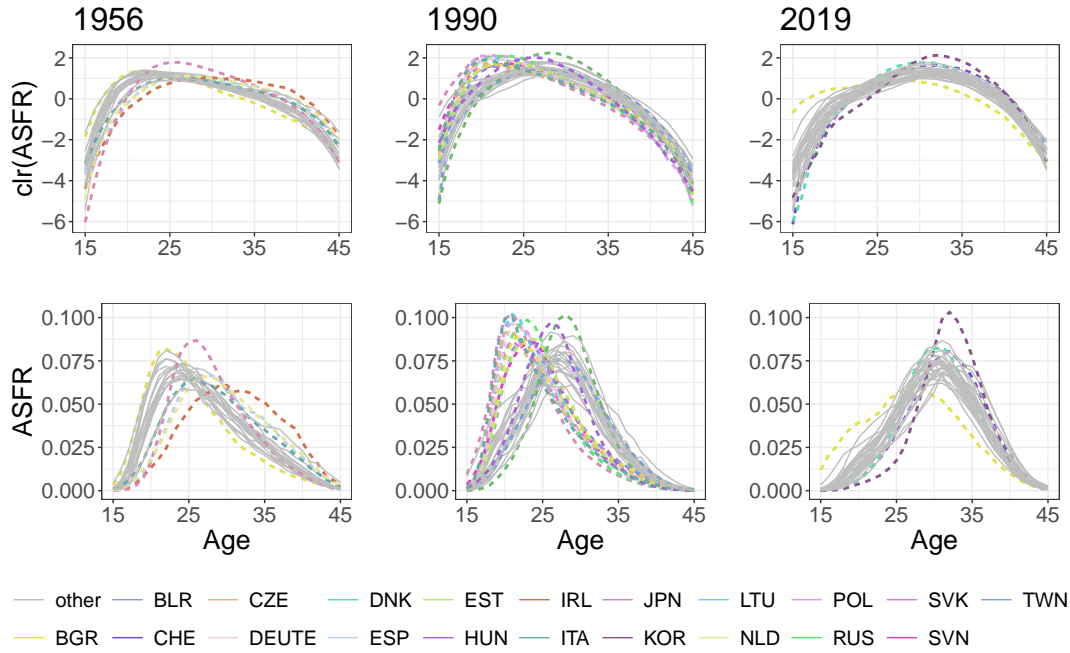


Figure 10: Fertility densities (lower row) and clr transformed densities (upper row) corresponding to years 1956, 1990, and 2019. Curves identified as outlying by Algorithm 1 are displayed as dashed lines.

tails of the densities. Here, the principal functions focus on the left tail and the following ages until the early 20s. The second principal function contains significantly less information mainly explaining the right tail and the peak fertility.

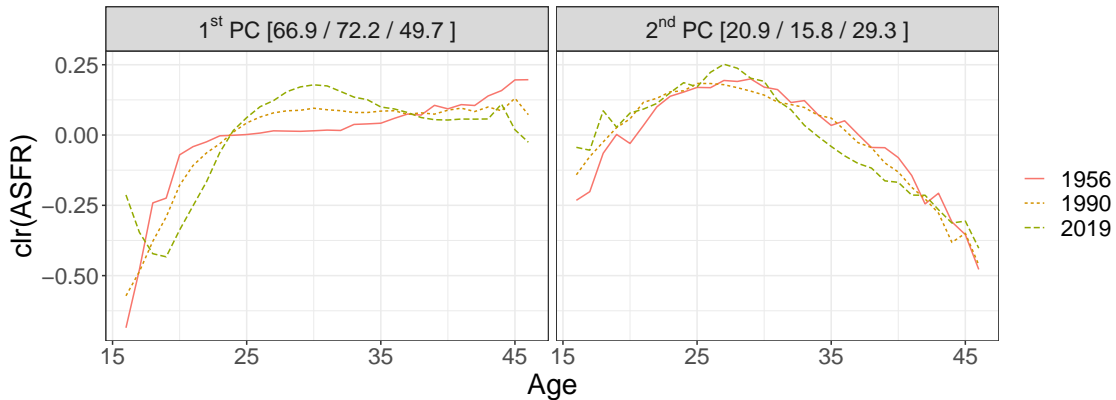


Figure 11: Comparison between the first two robust principal functions of the fertility data for years 1956, 1990, 2019. Corresponding percentage of explained variance in brackets (left to right).

Following the construction of robust principal components, we look at the corresponding estimated principal component scores \hat{s}_j associated with each country. In Figure 12 the first two robust scores for each country are visualized. For 1956 the outliers, as indicated by the triangles, all lay at the border of the data cloud. For Japan, both scores are exceedingly high, indicating not only relatively low fertility in younger age groups but also proportionally very high peak fertility. For the outliers of 1990 and 2019, we obtain a similar picture dominated by mostly extreme scores. For 1990 this mainly reflects countries that have a very early peak fertility. Similarly, in 2019 these extreme values explain high fertility rates at younger ages as well as late peak fertility.

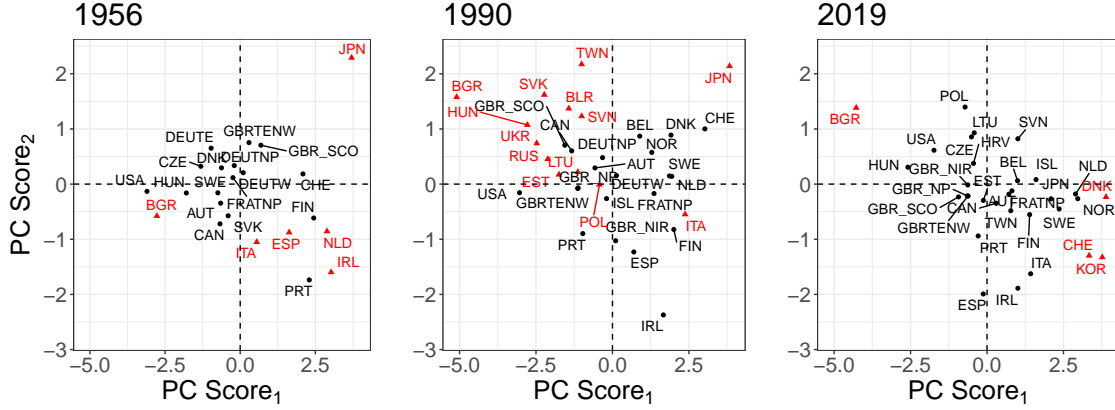


Figure 12: Robust principal component scores for the first and second eigenfunction for the years 1956, 1990, 2019 (from left to right). Circles correspond to regular observations while the triangles indicate outlying countries.

7 Conclusions and discussion

Despite the attention that the Bayes space methodology for density data analysis has attracted over the last decades, little focus has been paid to robust frameworks necessary for meaningful analysis in the presence of anomalies. Therefore, this paper introduces robust density PCA (RDPCA) as a methodology to robustly estimate the covariance operator and functional principal components of densely sampled univariate density data. Within this newly proposed method, we extend the notion of a functional Mahalanobis distance (Berrendero et al., 2020; Galeano et al., 2015) to the Bayes space. The resulting regularized Mahalanobis distance (RDMD) leads to a robust covariance estimation based on a subsample of those curves that best fit the underlying distribution. Based on this estimate, robust PCs for density function can be determined as summarized in Algorithm 1. During simulations, we demonstrated the efficiency of RDPCA as well as the advantages it has against a non-robust approach in the presence of outliers. Furthermore, if outliers arise within the tails of the densities, the clr transformation can amplify these deviations. Especially in these scenarios, we observed that common robust procedures that do not respect the nature of the data would fail.

One of our initial assumptions was that the data had been observed at a dense grid. In the case where the data is only available at a sparse grid, further extensions would require smoothing by an appropriate basis, e.g., CB-splines (Machalová et al., 2021) specifically developed for Bayes spaces. Naturally, the next step from univariate data would be to consider multivariate densities. During multivariate functional data analysis, each observation contains the recording of several “functional” variables. In this setting, not only the covariance between different time points is considered, but also the relation between individual variables. If the second dimension is also continuously observed, the observations are so-called random surfaces. As these statistical fields show increasingly practical relevance (Berrendero et al. (2011); Górecki et al. (2018); Dai and Genton (2018); Masak and Panaretos (2023) and references therein), expanding RDPCA to these areas seems worthwhile. Calculating the RDMD involved regularizing by a suitable operator that smooths out unwanted noise components while keeping the relevant signal within the (uncontaminated) data unaffected. Another class of meaningful operators that utilize the functional nature of the data are differential operators often used in Tikhonov regularization. One has to keep in mind that these operations have yet to be defined for Bayes spaces. Next to PCA, the regularized Mahalanobis distance could be used for concepts like linear or quadratic discriminant analysis for the classification density data. As these methods rely on similarity measures involving several covariance operators, the robust classification of densities based on the RDMD would be suitable.

Supplementary material

The supplement contains 3 sections. Within Section 1, we provide additional simulation results corresponding to Section 5.1 and 5.2 of this work. In Section 2, further results of the analysis of the fertility data in Section 6.2 are supplied. Section 3 finishes with the proofs.

Acknowledgement

The authors acknowledge support from the Austrian Science Fund (FWF), project number I 5799-N.

Disclosure statement

The authors report there are no competing interests to declare.

References

- Arribas-Gil, A. and J. Romo (2014, 03). Shape outlier detection and visualization for functional data: the Outliergram. *Biostatistics* 15(4), 603–619.
- Beaujouan, E. (2020). Latest-late fertility? Decline and resurgence of late parenthood across the low-fertility countries. *Population and Development Review* 46(2), 219–247.
- Berrendero, J. R., B. Bueno-Larraz, and A. Cuevas (2020). On Mahalanobis distance in functional settings. *Journal of Machine Learning Research* 21(9), 1–33.
- Berrendero, J. R., A. Justel, and M. Svarc (2011). Principal components for multivariate functional data. *Computational Statistics & Data Analysis* 55(9), 2619–2634.
- Boudt, K., P. J. Rousseeuw, S. Vanduffel, and T. Verdonck (2020). The minimum regularized covariance determinant estimator. *Statistics and Computing* 30(1), 113–128.
- Chakraborty, A. and P. Chaudhuri (2014). The spatial distribution in infinite dimensional spaces and related quantiles and depths. *The Annals of Statistics* 42(3), 1203 – 1231.
- Dai, W. and M. G. Genton (2018). Multivariate functional data visualization and outlier detection. *Journal of Computational and Graphical Statistics* 27(4), 923–934.
- Delicado, P. (2011). Dimensionality reduction when data are density functions. *Computational Statistics & Data Analysis* 55(1), 401–420.
- Egozcue, J. J., J. L. Díaz-Barrero, and V. Pawlowsky-Glahn (2006). Hilbert space of probability density functions based on Aitchison geometry. *Acta Mathematica Sinica* 22(4), 1175–1182.
- Febrero, M., P. Galeano, and W. González-Manteiga (2008). Outlier detection in functional data by depth measures, with application to identify abnormal NOx levels. *Environmetrics* 19(4), 331–345.
- Fraiman, R. and G. Muniz (2001, Dec). Trimmed means for functional data. *Test* 10(2), 419–440.
- Friedman, J. H. (1987). Exploratory Projection Pursuit. *Journal of the American Statistical Association* 82(397), 249–266.
- Galeano, P., E. Joseph, and R. E. Lillo (2015). The Mahalanobis Distance for Functional Data With Applications to Classification. *Technometrics* 57(2), 281–291.
- Ghiglietti, A., F. Ieva, and A. M. Paganoni (2017). Statistical inference for stochastic processes: two-sample hypothesis tests. *Journal of Statistical Planning and Inference* 180, 49–68.
- Górecki, T., M. Krzyśko, Ł. Waszak, and W. Wołyński (2018, Mar). Selected statistical methods of data analysis for multivariate functional data. *Statistical Papers* 59(1), 153–182.
- Hron, K., A. Menafoglio, M. Templ, K. Hrušová, and P. Filzmoser (2016). Simplicial principal component analysis for density functions in Bayes spaces. *Computational Statistics & Data Analysis* 94, 330–350.
- Kessy, A., A. Lewin, and K. Strimmer (2018). Optimal whitening and decorrelation. *The American Statistician* 72(4), 309–314.
- Kokoszka, P. and M. Reimherr (2017). *Introduction to Functional Data Analysis*. Chapman & Hall / CRC numerical analysis and scientific computing. CRC Press.
- Lemberge, P., I. Raedt, K. Janssens, F. Wei, and P. Van Espen (2000). Quantitative analysis of 16-17th century archaeological glass vessels using PLS regression of EPXMA and μ -XRF data. *Journal of Chemometrics* 14, 751–763.
- Locker, J. and P. Prenter (1980). Regularization with differential operators. I. General theory. *Journal of Mathematical analysis and applications* 74(2), 504–529.
- López-Pintado, S. and J. Romo (2009). On the concept of depth for functional data. *Journal of the American Statistical Association* 104(486), 718–734.
- Machalová, J., R. Talská, K. Hron, and A. Gába (2021, Jun). Compositional splines for representation of density functions. *Computational Statistics* 36(2), 1031–1064.

- Masak, T. and V. M. Panaretos (2023). Random surface covariance estimation by shifted partial tracing. *Journal of the American Statistical Association* 118(544), 2562–2574.
- Menafoglio, A., M. Grasso, P. Secchi, and B. M. Colosimo (2018). Profile monitoring of probability density functions via simplicial functional pca with application to image data. *Technometrics* 60(4), 497–510.
- Menafoglio, A., L. Guadagnini, A. Guadagnini, and P. Secchi (2021). Object oriented spatial analysis of natural concentration levels of chemical species in regional-scale aquifers. *Spatial Statistics* 43, 100494.
- Morigi, S., L. Reichel, and F. Sgallari (2007). Orthogonal projection regularization operators. *Numerical Algorithms* 44(2), 99–114.
- Nagler, T. (2024). *kde1d: Univariate Kernel Density Estimation*. R package version 1.0.7, <https://cran.r-project.org/web/packages/kde1d/index.html>.
- Oguamalam, J., U. Radojičić, and P. Filzmoser (2024). Minimum regularized covariance trace estimator and outlier detection for functional data. *Technometrics* 66(4), 588–599.
- Oja, H., S. Sirkiä, and J. Eriksson (2016). Scatter matrices and independent component analysis. *Austrian Journal of Statistics* 35, 175–189.
- Ostebee, A. and P. Zorn (2002). *Calculus from Graphical, Numerical, and Symbolic Points of View*. Number Bd. 2 in *Calculus from Graphical, Numerical, and Symbolic Points of View*. Harcourt College Publishers.
- Pawlowsky-Glahn, V., J. Egozcue, and R. Tolosana-Delgado (2015). *Modeling and analysis of compositional data*. Wiley, Chichester.
- Petersen, A., C. Zhang, and P. Kokoszka (2022). Modeling probability density functions as data objects. *Econometrics and Statistics* 21, 159–178.
- Ramsay, J. O. and B. W. Silverman (1997). *Principal components analysis for functional data*. New York, NY: Springer New York.
- Ramsay, J. O. and B. W. Silverman (2005). *Functional Data Analysis*. Springer.
- Rousseeuw, P. J. and K. V. Driessen (1999). A fast algorithm for the minimum covariance determinant estimator. *Technometrics* 41(3), 212–223.
- Secchi, P., A. Stamm, and S. Vantini (2013). Inference for the mean of large p small n data: A finite-sample high-dimensional generalization of Hotelling’s theorem. *Electronic Journal of Statistics* 7(none), 2005 – 2031.
- Talská, R., A. Menafoglio, K. Hron, J. J. Egozcue, and J. Palarea-Albaladejo (2020). Weighting the domain of probability densities in functional data analysis. *Stat* 9(1), e283. e283 sta4.283.
- van den Boogaart, K.-G., J. J. Egozcue, and V. Pawlowsky-Glahn (2010). Bayes linear spaces. *SORT : statistics and operations research transactions* 34(2), 201–222.
- van den Boogaart, K.-G., V. Pawlowsky-Glahn, and J. J. Egozcue (2014). Bayes Hilbert spaces. *Australian & New Zealand Journal of Statistics* 56, 171–194.
- Wang, Z. (2012). Multi-parameter Tikhonov regularization and model function approach to the damped Morozov principle for choosing regularization parameters. *Journal of Computational and Applied Mathematics* 236(7), 1815–1832.

SUPPLEMENT OF: ROBUST FUNCTIONAL PCA FOR DENSITY DATA

A PREPRINT

✉ **Jeremy Oguamalam***

Institute of Statistics and Mathematical Methods in Economics
TU Wien
Vienna, Austria

✉ **Peter Filzmoser**

Institute of Statistics and Mathematical Methods in Economics
TU Wien
Vienna, Austria

✉ **Karel Hron**

Department of Mathematics and Statistics
Palacký University Olomouc
Olomouc, Czechia

✉ **Alessandra Menafoglio**

Department of Mathematics
Politecnico di Milano
Milan, Italy

✉ **Una Radojčić**

Institute of Statistics and Mathematical Methods in Economics
TU Wien
Vienna, Austria

January 3, 2025

1 Simulations

1.1 Simulation 1

In this section, we extend the simulation of Section 5.1 by

Model 1.2 : $X_{\text{reg}} = \text{KDE}(Y_1, \dots, Y_N)$, $X_{\text{out}} = \text{KDE}(Y_1, \dots, Y_N, \tilde{Y}_1, \dots, \tilde{Y}_{\lfloor 0.05N \rfloor})$, and

Model 1.3 : $X_{\text{reg}} = \text{KDE}(Z_1, \dots, Z_N)$, $X_{\text{out}} = \text{KDE}(Z_1, \dots, Z_N, \tilde{Z}_1, \dots, \tilde{Z}_{\lfloor 0.1N \rfloor})$.

For Model 1.2 we have $Y_i \sim N(0, 1)$, $\tilde{Y}_i \sim U([q_1; q_2])$, $N = 250$, with q_1, q_2 being the 0.01% and 0.25% quantile of the standard normal distribution, while for 1.3 we set $Z_i \sim \chi_6^2$, $\tilde{Z}_i \sim U([q_3; q_4])$, and q_3, q_4 to the 0.1% and 0.2% quantiles of χ_6^2 . To showcase the densities and the clr transformed curves, we provide Figure 1.

Both settings were analyzed for the same parameter configurations of c, α, h , and k as in Section 5.1. We evaluate the performance of RDPCA and compare it to SFPCA using two statistical measures. The integrated square error (ISE) measures the accuracy between an estimate of true underlying covariance and the covariance based on the robust/non-robust approach. Precisely, given estimates $\hat{v}, \hat{\gamma}$ of the covariance function, the ISE is defined as $\text{ISE} = p^{-2} \sum_{i,j=1}^p (\hat{\gamma}(t_i, t_j) - \hat{v}(t_i, t_j))^2$. The estimate of the true covariance is based on the sample covariance of a Monte Carlo simulation where many samples following the true distribution are generated. The corresponding results are shown in Figure 2. This is followed by the mean cosine between the first five pairs of eigenfunctions based on estimated covariance and the true covariance. These values are depicted in the bottom of Figure 2. Similar as during the initial presentation of this simulation in Section 5.1, both the ISE and the mean cosine indicate that RDPCA outperforms SFPCA when outliers are present.

*The authors gratefully acknowledge support from the Austrian Science Fund (FWF), project number I 5799-N

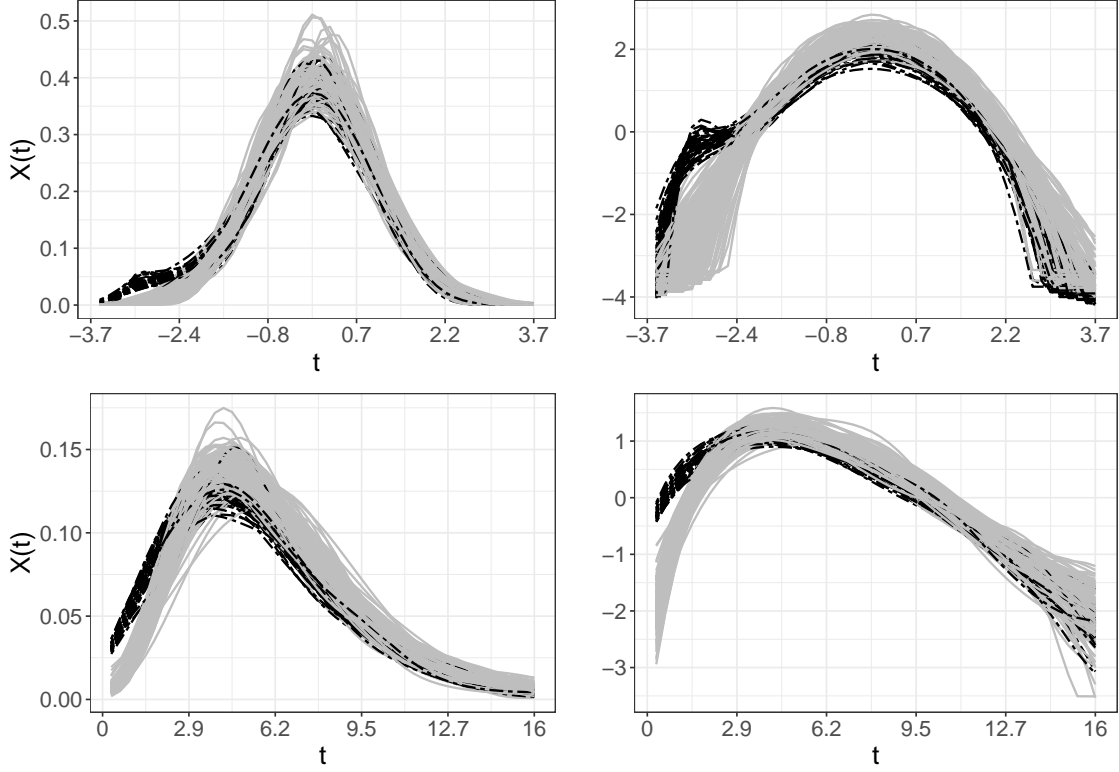


Figure 1: Visualization of densities (left) and clr transformed densities (right) for Model 1.2 (top row) and Model 1.3 (bottom row). Solid curves represent the main processes, while the dashed ones indicate the outliers. The sample size is $n = 200$, $p = 50$ time points, and the contamination rate is $c = 0.2$.

Finally, we evaluate the advantage of the clr transformation over a non-compositional, simple functional approach. As the clr transformation focuses on relative changes, rather than absolute differences, small deviations within the tails of the distribution carry significantly more weight after transforming the data. Based on the squared RDMD and α -Mahalanobis distances as well as the corresponding theoretical cutoff values, we can calculate true positive and true negative rates. In Figure 3 the resulting rates are presented. Model 1.1 refers to the model presented in Section 5.1. In situations where outliers differ in the tails of the domain, a direct approach would completely fail in correctly distinguishing regular and irregular observations from each other. Thus, when analyzing density data, the clr transformation can be an important and necessary tool to emphasize the relative scale property.

1.2 Simulation 2

In the extension of the second simulation study, we construct data by

$$\begin{aligned} \text{Model 2.2: } \text{clr}(X_{\text{reg}}(t)) &= s_1\xi_1 + s_2\xi_2 + s_3\xi_3 + s_4\xi_4, \\ \text{clr}(X_{\text{out}}(t)) &= \tilde{s}_1\xi_1 + \tilde{s}_2\xi_2 + \tilde{s}_3\xi_3 + \tilde{s}_4\xi_4 \end{aligned}$$

for the eigenfunctions $\xi_1(t) = \sqrt{2}\sin(2\pi t)$, $\xi_2(t) = \sqrt{2}\cos(2\pi t)$, $\xi_3(t) = \sqrt{2}\sin(4\pi t)$, $\xi_4(t) = \sqrt{2}\cos(4\pi t)$ of the covariance operator of the clr transformed densities. The corresponding scores satisfy $\mathbb{E}[s_j] = 0$ while $\text{var}(s_j)$ is equal to the j -th eigenvalue λ_j of the covariance operator. By Mercer's Theorem (Kokoszka and Reimherr, 2017) the covariance function satisfies $\gamma(s, t) = \sum_{j=1}^4 s_j\xi_j(s)\xi_j(t)$.

To showcase Model 2.2, we provide Figure 4. In this setting, the outlying scores follow a different distribution than the scores corresponding to regular observations. As in Section 5.2, the regular scores either individually follow an independent normal distribution, i.e. $s_i \sim N(0, \lambda_i)$ or jointly a multivariate t-distribution, i.e. $(s_1, s_2, s_3, s_4) \sim t_5(\mathbf{0}, \text{diag}(\lambda_1, \lambda_2, \lambda_3\lambda_4))$ with $(\lambda_1, \lambda_2, \lambda_3\lambda_4) = (2, 1, 1/2, 1/4)$. Scores \tilde{s}_i of the outlying curves follow the same scheme under different scaling parameters $(\tilde{\lambda}_1, \tilde{\lambda}_2, \tilde{\lambda}_3\tilde{\lambda}_4) = (4, 3, 5/2, 9/4)$.

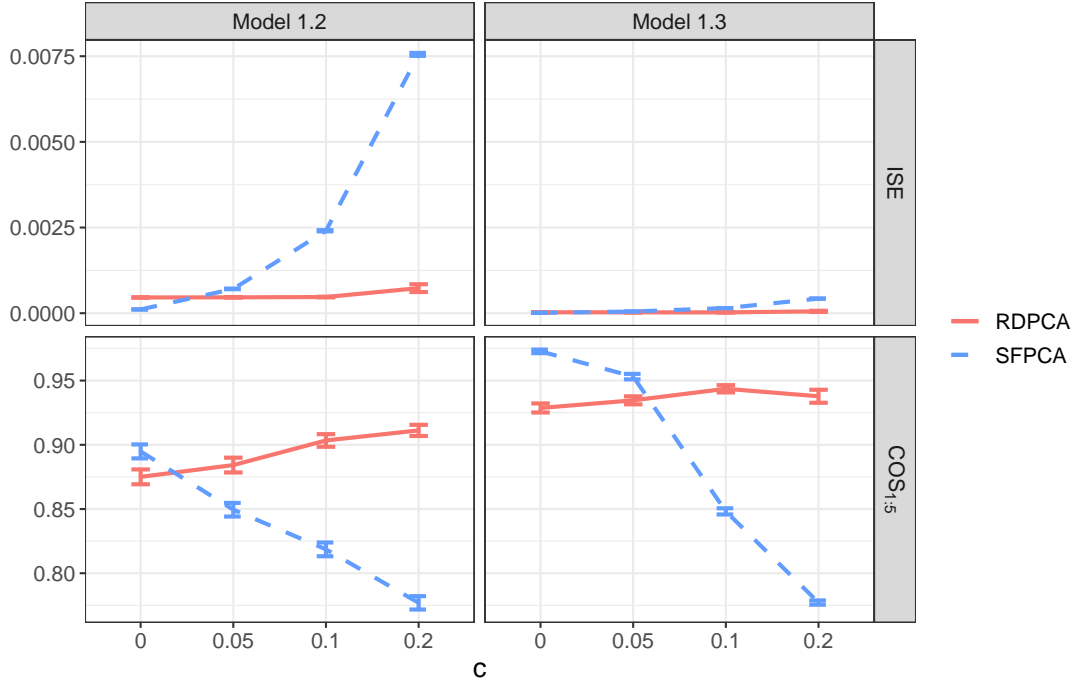


Figure 2: Integrated square error and mean cosine between estimated and true eigenfunctions. Displayed are the mean \pm one standard error of each measure over all iterations at each level of the corresponding parameter configuration. Top row: ISE. Bottom row: Mean Cosine between the first five pairs of eigenfunctions. All measurements are calculated based on the covariance estimated on RDPCA (solid) and SFPCA (dashed) and respectively compared with a sample estimate based on a Monte Carlo simulation of the true distribution.

As in the previous simulation, this analysis also considers varying contamination rates, i.e. $c = \{0, 0.05, 0.1, 0.2\}$, an automatically selected regularization parameter α , and $h = \lceil 0.75n \rceil$, $k = 1$. Each parameter configuration is iterated 100 times. Also, the performance is measured by the ISE, the mean cosine of the first four pair of eigenfunctions and compared to SFPCA. The corresponding results are shown in the left part of Figure 5. On the right is the mean cosine based on the estimated covariance and the true covariance. Both measures suggest that the robust approach performs similar or even better than the non-robust approach in the presence of outliers.

Another important feature is the accuracy of the estimation of the eigenvalues λ_j . To measure this performance consider the explained variance of the first five estimated eigenfunctions. These results are depicted in Figure 6 where we compare the ratio of explained variance to the true proportion for a contamination rate of $c = 0.2$. The results clearly show that only RDPCA can precisely identify the correct ratios for all estimated eigenfunctions.

2 Real-data example

2.1 Fertility data

In this section more details around the analysis of the fertility data from the Human Fertility Database (HFD) in Section 6.2 is provided. At the time of this analysis, the HFD provides age-specific fertility rates (ASFR) for 39 countries spanning from 1891 to 2023. To ensure reliable analysis, we focus on years where data for at least 20 countries is available, narrowing our time frame to 1955-2020. We further preprocess the data by concentrating on the age groups from 15 to 45 years, resulting in $p = 31$ age groups. This focus is justified by biological and statistical considerations: this age range captures the majority of female reproductive years, and fertility rates outside this range are significantly lower and more subjective to extreme variability.

For each year, we are applying RDPCA to the resulting ASFR data, using parameters $k = 1$, $h = \lceil 0.5n \rceil$, and selecting α automatically. It is important to note that not all countries have data continuously available across all years.

In Figure 7, we summarize the yearly evolution of the outlying behavior between 1955 and 2020 over all countries. In the first half of the observed time period, we primarily get persistent outliers like Spain (ESP) and Portugal (PRT) or the

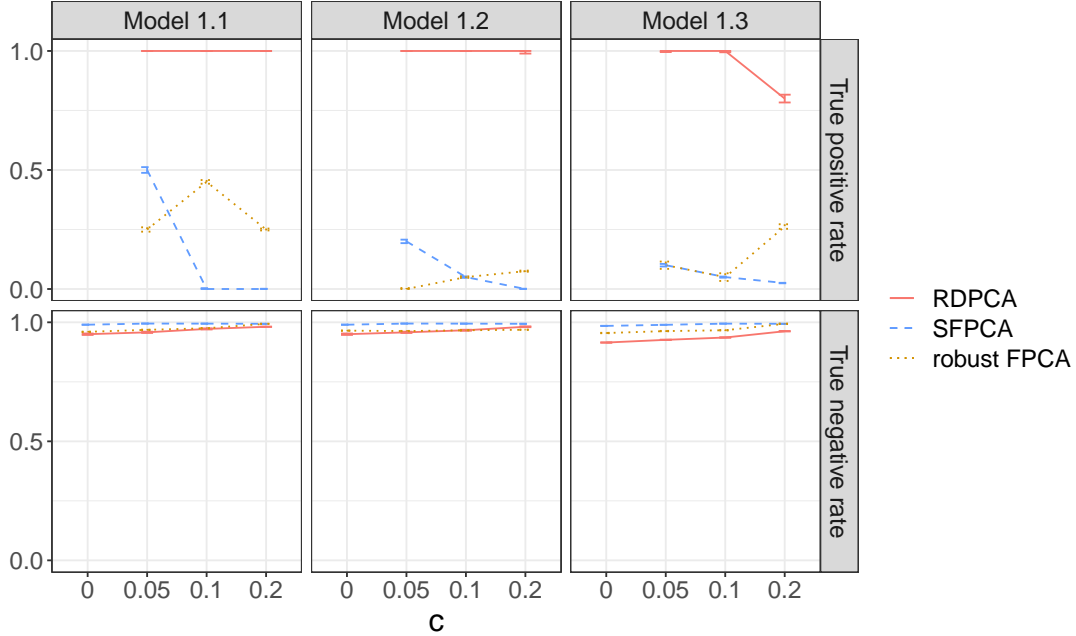


Figure 3: True positive and true negative rate of models of the first simulation, comparing RDPCA, SFPCA, and robust FPCA. Displayed are the mean \pm one standard error over all iterations at each level of the corresponding parameter configuration.

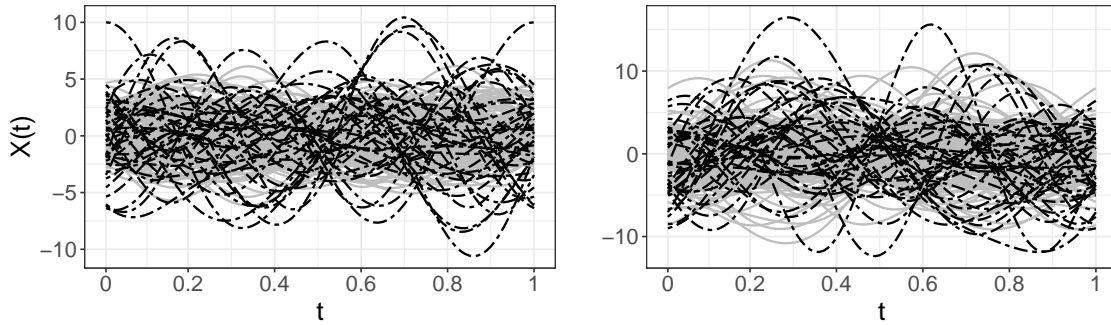


Figure 4: Visualization of curves for Model 2.2 with normal (left) and multivariate t-distributed (right) scores. Solid curves represent the main processes, dashed ones indicate outliers. Parameters: $n = 200$, $p = 100$, $c = 0.2$.

Czech Republic (CZE) and Japan (JPN). For some of these countries, the reason why they behave outlying are their outstandingly late (first-) pregnancies. Amongst others, this was caused by economic uncertainties, large families, and children tending to stay longer at home before moving out. As opposed to this, rather early parenthood, influenced by the Soviet Union was present in the Czech Republic. During the more recent years countries like Russia (RUS), Belarus (BLR) and the Ukraine (UKR) exhibit and outlying behavior. As discussed above, overall pregnancies shifted from younger to higher ages due to several reasons. Within East Europe, especially for the latter countries, this trend was delayed and is partially still ongoing.

As it was already shown in Section 6.2, the first principal function mainly captures information contained in the left tail. A closer look to the complete period in Figure 8 reveals an interesting dynamic around the 90s. During that time, high fertility in western countries within Europe shifted earlier compared to the East. This is displayed by the shape of the principal functions that exhibit two extrema, representing the East and the West, respectively. On the other hand, the simplicial principal components fail to capture this trend at all. There is no apparent change over the consulted period.

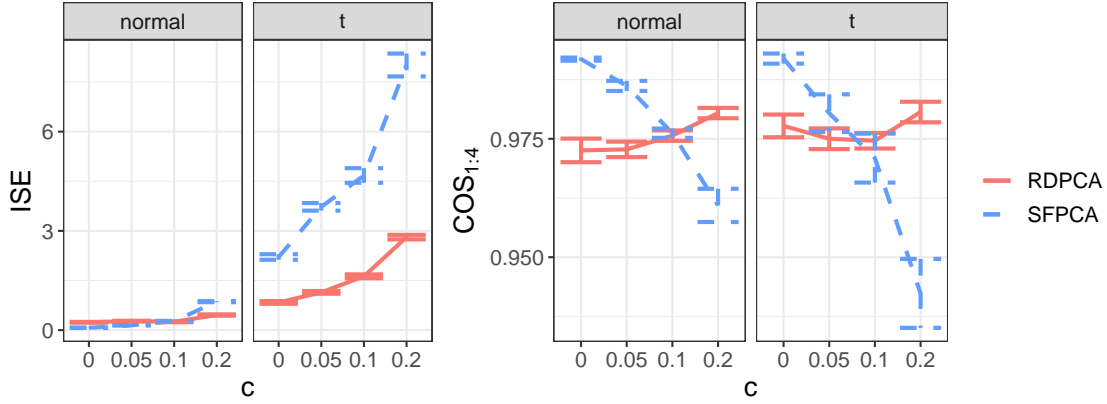


Figure 5: Integrated square error and cosine between first four pairs of estimated and true eigenfunctions. Displayed are the mean \pm one standard error of each measure over all iterations at each level of the corresponding parameter configuration. All measurements are calculated based on RDPCA and SFPCA covariance estimators and respectively compared with a true covariance function $\gamma(s, t) = \sum_{j=1}^4 s_j \xi_j(s) \xi_j(t)$. The notation “normal” and “t” refer to the distribution of the scores in the underlying model as described at the beginning of this section.

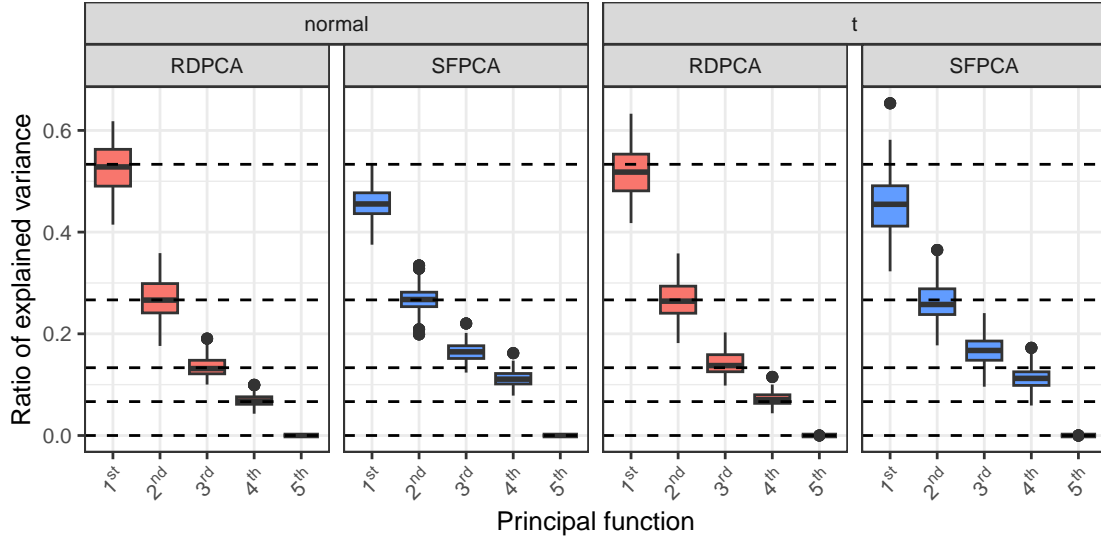


Figure 6: Estimated ratio of explained variance for the first five principal functions over different score distributions at $c = 0.2$. The dashed reference lines depict the true proportion.

3 Proofs

Proof 3.1 (Proof of Lemma 2.1)

i) Observe first that the Bayes mean $\mu_{B^2, X}$ is connected to the “standard” mean of $\text{clr}(X)$ through:

$$\begin{aligned} \langle \text{clr}(\mu_{B^2, X}), \text{clr}(f) \rangle &= \langle \mu_{B^2, X}, f \rangle_{B^2} = \mathbb{E}(\langle X, f \rangle_{B^2}) \\ &= \mathbb{E}(\langle \text{clr}(X), \text{clr}(f) \rangle) = \langle \mathbb{E}(\text{clr}(X)), \text{clr}(f) \rangle, \end{aligned} \quad (1)$$

where the last equality holds since $\mathbb{E}(\text{clr}(X))$ is the expectation of $\text{clr}(X)$. Moreover, for a constant function $g \equiv c \in \mathbb{R}$

$$\langle \text{clr}(\mu_{B^2, X}), g \rangle = 0, \quad \langle \mathbb{E}(\text{clr}(X)), g \rangle = \mathbb{E}(\langle \text{clr}(X), g \rangle) = 0.$$

Additionally, (1) shows that $\text{clr}(\mu_{B^2, X})$ and $\mathbb{E}(\text{clr}(X))$ coincide on projections onto every $f_0 \in L_0(I)$. As every function $f \in L^2(I)$ can be written as $f = f_0 + c_f$, where $c_f = \int_I f(t) dt$ and $f_0 \in L_0(I)$, we deduce that $\text{clr}(\mu_{B^2, X})$ and $\mathbb{E}(\text{clr}(X))$ coincide on projections onto every $f \in L(I)$, thus proving the first claim.



Figure 7: Yearly evolution of anomaly detection within fertility curves.

ii) The following identity connecting the Bayes covariance of X and standard, L^2 covariance of $\text{clr}(X)$ holds: For $f, g \in \mathcal{B}^2(I)$

$$\begin{aligned} \langle \text{clr}(C_{B^2, X} f), \text{clr}(g) \rangle &= \langle C_{B^2, X} f, g \rangle_{B^2} = \mathbb{E} \left(\langle X \ominus \mu_{B^2, X}, f \rangle_{B^2} \langle X \ominus \mu_{B^2, X}, g \rangle_{B^2} \right) \\ &= \mathbb{E} \left(\langle \text{clr}(X) - \mathbb{E}(X), \text{clr}(f) \rangle \langle \text{clr}(X) - \mathbb{E}(X), \text{clr}(g) \rangle \right) \\ &= \langle C_{\text{clr}(X)} \text{clr}(f), \text{clr}(g) \rangle, \end{aligned}$$

thus proving that $\text{clr}(C_{B^2, X} f)$ and $C_{\text{clr}(X)} \text{clr}(f)$ coincide on projections in L_0 . Using the same argument as for the expectation, we obtain that for every $f \in \mathcal{B}^2(I)$

$$\text{clr}(C_{B^2, X} f) =_{a.e.} C_{\text{clr}(X)} \text{clr}(f).$$

iii) This statement is a direct consequence of (ii) and the definition of Bayes space inner product.

Proof 3.2 (Proof of Proposition 3.1) Using the definition of Bayes-space norm and clr transformation we first obtain that

$$\begin{aligned} \text{clr}(C_{B^2, X}^{1/2} Y) &= \text{clr} \left(\bigoplus_{i=1}^{\infty} (\lambda_i^{1/2} \langle \zeta_i, Y \rangle_{B^2}) \odot \zeta_i \right) = \sum_{i=1}^{\infty} \lambda_i^{1/2} \langle \zeta_i, Y \rangle_{B^2} \text{clr}(\zeta_i) \\ &= \sum_{i=1}^{\infty} \lambda_i^{1/2} \langle \text{clr}(\zeta_i), \text{clr}(Y) \rangle_{L^2} \text{clr}(\zeta_i) \end{aligned} \quad (2)$$

for (λ_i, ζ_i) , $i \geq 1$ being the i th eigenpair of $C_{B^2, X}$. Additionally, Lemma 2.1 gives that

$$\sum_{i=1}^{\infty} \lambda_i^{1/2} \langle \text{clr}(\zeta_i), \text{clr}(Y) \rangle_{L^2} \text{clr}(\zeta_i) = C_{\text{clr}, X}^{1/2} \text{clr}(Y). \quad (3)$$

(2) and (3), together with the definition of the Bayes-space norm finally give that

$$\arg \min_{Y \in \mathcal{B}^2(I)} \left\{ \|C_{B^2, X}^{1/2} Y \ominus X\|_{B^2}^2 + \alpha \|Y\|_{B^2}^2 \right\} = \arg \min_{Y \in \mathcal{B}^2(I)} \left\{ \|C_{\text{clr}, X}^{1/2} \text{clr}(Y) - \text{clr}(X)\|^2 + \alpha \|\text{clr}(Y)\|^2 \right\}. \quad (4)$$

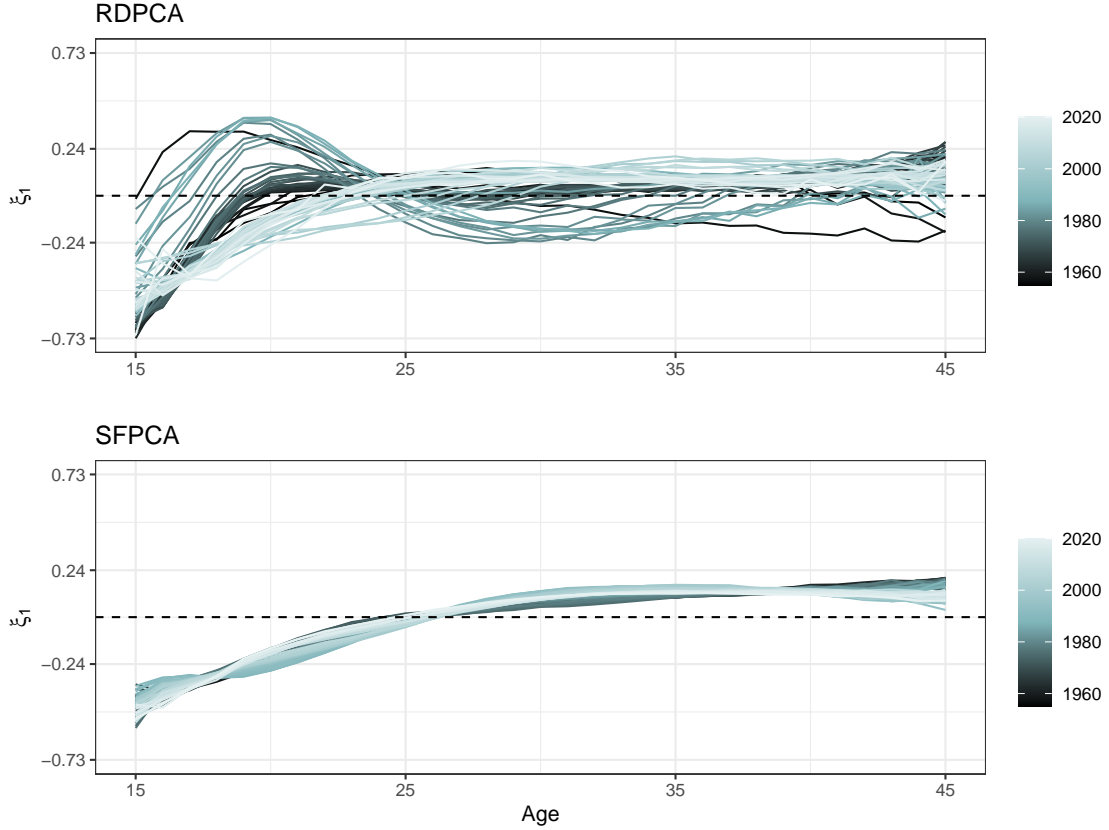


Figure 8: First principal function for fertility curves over the years 1955 until 2020.

Let now

$$X_{\text{st}}^{\alpha, I} =_B \arg \min_{Y \in \mathcal{B}^2(I)} \left\{ \|C_{\mathcal{B}^2, X}^{1/2} Y \ominus X\|_{\mathcal{B}}^2 + \alpha \|Y\|_{\mathcal{B}}^2 \right\}. \quad (5)$$

Denoting $L_0^2(I) \subset L^2(I)$ to be the set of all clr-transformed elements of $\mathcal{B}^2(I)$, i.e. the set of L^2 -functions with zero internal, (4) then allows us to reparameterize the optimization problem (5) as

$$X_{\text{st}}^{\alpha, I} =_B \text{clr}^{-1}(Y), \quad Y = \arg \min_{Z \in L_0^2(I)} \left\{ \|C_{\text{clr}, X}^{1/2} Z - \text{clr}(X)\|^2 + \alpha \|Z\|^2 \right\}.$$

We now need to show that

$$\arg \min_{Y \in L_0^2(I)} \left\{ \|C_{\text{clr}, X}^{1/2} Y - \text{clr}(X)\|^2 + \alpha \|Y\|^2 \right\} = \arg \min_{Y \in L^2(I)} \left\{ \|C_{\text{clr}, X}^{1/2} Y - \text{clr}(X)\|^2 + \alpha \|Y\|^2 \right\}.$$

We know that

$$\arg \min_{Y \in L^2(I)} \left\{ \|C_{\text{clr}, X}^{1/2} Y - \text{clr}(X)\|^2 + \alpha \|Y\|^2 \right\} = C_{\text{clr}, X}^{1/2} (C_{\text{clr}, X} + \alpha I) \text{clr}(X) =: Y_{L^2};$$

see e.g. Berrendero et al. (2020) for more details. Linearity of the integral implies that $Y_{L^2} \in L_0^2(I)$, thus completing the first part of the proof. The other implication is shown using analogously.

Proof 3.3 (Proof of Corollary 3.1) Proposition 3.1 implies that it is enough to show that

$$\text{clr} \left(\bigoplus_{i=1}^{\infty} \frac{\lambda_i^{1/2}}{\lambda_i + \alpha} \odot \langle \zeta_i, X \rangle_{\mathcal{B}^2} \odot \zeta_i \right)$$

solves the equivalent optimization problem in L^2 . Properties of Bayes space norm and operations give that

$$\begin{aligned} \text{clr} \left(\bigoplus_{i=1}^{\infty} \frac{\lambda_i^{1/2}}{\lambda_i + \alpha} \odot \langle \zeta_i, X \rangle_{B^2} \odot \zeta_i \right) &= \sum_{i=1}^{\infty} \frac{\lambda_i^{1/2}}{\lambda_i + \alpha} \langle \text{clr}(\zeta_i), \text{clr}(X) \rangle \text{clr}(\zeta_i) \\ &= C_{\text{clr}, X}^{1/2} (C_{\text{clr}, X} + \alpha I)^{-1} \text{clr}(X), \end{aligned}$$

which is an optimizer of the equivalent optimization problem in L^2 ; see the final part of the proof of Proposition 3.1 for more insight.

Proof 3.4 (Proof of Proposition 3.2) As $\tilde{X} \in \mathcal{N}(L)$, the minimization problem in the statement of the proposition can be rewritten as

$$\arg \min_{Y \in \mathcal{B}^2(I)} \left\{ \|C_{B^2, X}^{1/2} (Y \ominus \tilde{X}) \ominus X\|_{B^2}^2 + \alpha \|L(Y - \tilde{X})\|_{B^2}^2 \right\},$$

admitting a unique solution in the form $Y \ominus \tilde{X} = X_{\text{st}}^{\alpha, L}$.

Proof 3.5 (Proof of Proposition 3.3) The equivalence between the two optimization problems is shown as in the proof of Proposition (3.1). We next show that the optimization problem in a Bayes space has an explicit solution. Denote first $W(-k)$ to be the orthogonal projector onto the span $\text{span}(\zeta_1, \dots, \zeta_k)$ of the first k eigenfunctions of X . Then, for every $Y \in \mathcal{B}^2(I)$, we can write $Y = W(-k)Y \oplus W(k)Y$. This further allows us to rewrite

$$\begin{aligned} X_{\text{st}; C_{B^2, X}}^{\alpha, k} &=_{\mathcal{B}} \arg \min_{Y \in \mathcal{B}^2(I)} \left\{ \left\| \left(C_{B^2, X}^{1/2} W(k)Y \ominus W(k)X \right) \oplus \left(C_{B^2, X}^{1/2} W(-k)Y \ominus W(-k)X \right) \right\|_{\mathcal{B}}^2 \right. \\ &\quad \left. + \alpha \|W(k)Y\|_{\mathcal{B}}^2 \right\}. \end{aligned}$$

As $W(k)C_{B^2, X}^{1/2}W(k)Y = C_{B^2, X}^{1/2}W(k)Y$ and $W(-k)C_{B^2, X}^{1/2}W(-k)Y = C_{B^2, X}^{1/2}W(-k)Y$ it follows that $C_{B^2, X}^{1/2}W(k)Y \ominus W(k)X$ and $C_{B^2, X}^{1/2}W(-k)Y \ominus W(-k)X$ are orthogonal in $\mathcal{B}^2(I)$. Thus,

$$\begin{aligned} X_{\text{st}; C_{B^2, X}}^{\alpha, k} &=_{\mathcal{B}} \arg \min_{Y \in \mathcal{B}^2(I)} \left\{ \|C_{B^2, X}^{1/2} W(k)Y \ominus W(k)X\|_{\mathcal{B}}^2 + \alpha \|W(k)Y\|_{\mathcal{B}}^2 \right. \\ &\quad \left. + \|C_{B^2, X}^{1/2} W(-k)Y \ominus W(-k)X\|_{\mathcal{B}}^2 \right\}. \end{aligned}$$

Observe now two optimization problems independently

$$\min_{Y_1 \in \mathcal{B}^2(I)} \left\{ \|C_{B^2, X}^{1/2} W(k)Y_1 \ominus W(k)X\|_{\mathcal{B}}^2 + \alpha \|Y_1\|_{\mathcal{B}}^2 \right\} \quad (6)$$

$$\min_{Y_2 \in \mathcal{B}^2(I)} \left\{ \|C_{B^2, X}^{1/2} W(-k)Y_2 \ominus W(-k)X\|_{\mathcal{B}}^2 \right\}. \quad (7)$$

Regularization in (6) is said to be in a standard form and admits a closed-form solution

$$\begin{aligned} Y_1 &=_{\mathcal{B}^2} C_{B^2, X}^{1/2} W(k) \left(C_{B^2, X}^{1/2} W(k) C_{B^2, X}^{1/2} + \alpha I \right)^{-1} W(k) X \\ &= \sum_{i=k+1}^{\infty} \frac{\lambda_i^{1/2}}{\lambda_i + \alpha} \langle \zeta_i, X \rangle_{B^2} \zeta_i \in \text{span}(\zeta_{k+1}, \zeta_{k+2}, \dots), \end{aligned}$$

see the proof of (Berrendero et al., 2020, Proposition 2) for more details. Additionally, since $C_{B^2, X}^{1/2} W(-k)$ is invertible, (6) has a solution

$$Y_2 = \sum_{i=1}^k \lambda_i^{-1/2} \langle \zeta_i, X \rangle_{B^2} \zeta_i \in \text{span}(\zeta_1, \dots, \zeta_k).$$

It is then straightforward to verify that $Y = Y_1 \oplus Y_2$ is the solution to the original optimization problem. Similarly, one can show that

$$\sum_{i=1}^k \lambda_i^{-1/2} \langle \text{clr}(X), \xi_i \rangle \xi_i + \sum_{i=k+1}^{\infty} \frac{\lambda_i^{1/2}}{\lambda_i + \alpha} \langle \text{clr}(X), \xi_i \rangle \xi_i$$

is a solution to the corresponding optimization problem in the clr space. From here, it is again straightforward to verify the equivalence of the corresponding optimization problems.

Proof 3.6 (Proof of Proposition 3.4) For simplicity, we give the proof for $k \geq 1$. The other case is shown using the same argumentation. As in the proof of Proposition 3.3 and using the definition of Bayes-space inner product, we obtain that

$$M_{\alpha,k,B^2}^2(X) = \sum_{i=1}^k \frac{1}{\lambda_i} z_i^2 + \sum_{i=k+1}^{\infty} \frac{\lambda_i}{(\lambda_i + \alpha)^2} z_i^2,$$

where $z_i = \langle \text{clr}(X), \xi_i \rangle$, $i \geq 1$. Gaussianity of $\text{clr}(X)$ gives that the scores $z_i \sim \mathcal{N}(0, \lambda_i)$, $i \geq 1$ are mutually independent. Substituting $\eta_i = \lambda_i^{-1/2} z_i$, $i \geq 1$ yields the desired claim.

Proof 3.7 (Proof of Proposition 3.5) Claim (i) follows directly from the (Berrendero et al., 2020, Proposition 2). Using the same reasoning

$$M_{\alpha,k,B^2}^2(X) = \sum_{i=1}^k \frac{\langle \text{clr}(X), \xi_i \rangle^2}{\lambda_i} + \sum_{i=k+1}^{\infty} \frac{\lambda_i}{(\lambda_i + \alpha)^2} \langle \text{clr}(X), \xi_i \rangle^2.$$

As $0 \leq \langle \text{clr}(X), \xi_i \rangle^2 \leq \|\text{clr}(X)\|^2$, we have that the second part in the upper sum is bounded by

$$0 \leq \sum_{i=k+1}^{\infty} \frac{\lambda_i}{(\lambda_i + \alpha)^2} \langle \text{clr}(X), \xi_i \rangle^2 \leq \|\text{clr}(X)\|^2 \sum_{i=k+1}^{\infty} \frac{\lambda_i}{(\lambda_i + \alpha)^2},$$

where the upper sequence converges uniformly for all $\alpha > 0$. Denoting $f(i, \alpha) = \frac{\lambda_i}{(\lambda_i + \alpha)^2}$, Hildebrandt (1912, Theorem 1) implies that the limit and sum commute. Additionally, as for every i $\lim_{\alpha \rightarrow \infty} f(i, \alpha) = 0$ gives

$$0 \leq \lim_{\alpha \rightarrow \infty} \sum_{i=k+1}^{\infty} \frac{\lambda_i}{(\lambda_i + \alpha)^2} \langle \text{clr}(X), \xi_i \rangle^2 \leq 0,$$

thus completing the proof if (ii).

Proof 3.8 (Proof of Corollary 4.1) We start this proof by showing $\|X_{\text{st}, \hat{C}_{B^2, X}}^{\alpha, k}\|_{B^2} \rightarrow_{\text{a.s.}} \|X_{\text{st}, C_{B^2, X}}^{\alpha, k}\|_{B^2}$. First, note that Proposition 3.3 further implies an explicit representation for the solution of (7) based on the underlying operators. From this, it follows, that

$$\begin{aligned} \|X_{\text{st}, \hat{C}_{B^2, X}}^{\alpha, k}\|_{B^2} - \|X_{\text{st}, C_{B^2, X}}^{\alpha, k}\|_{B^2} &\leq \|X_{\text{st}, \hat{C}_{B^2, X}}^{\alpha, k} \ominus X_{\text{st}, C_{B^2, X}}^{\alpha, k}\|_{B^2} \\ &= \|\hat{C}_{B^2, X}^{1/2} (\hat{C}_{B^2, X} \oplus \alpha \hat{W}(k))^{-1} (X \ominus \hat{\mu}_{B^2, X}) \\ &\quad \ominus C_{B^2, X}^{1/2} (C_{B^2, X} \oplus \alpha W(k))^{-1} X\|_{B^2} \\ &\leq \|\left(\hat{C}_{B^2, X}^{1/2} (\hat{C}_{B^2, X} \oplus \alpha \hat{W}(k))^{-1} \ominus C_{B^2, X}^{1/2} (C_{B^2, X} \oplus \alpha W(k))^{-1} \right) X\|_{B^2} \\ &\quad + \|\hat{C}_{B^2, X}^{1/2} (\hat{C}_{B^2, X} \oplus \alpha \hat{W}(k))^{-1} \hat{\mu}_{B^2, X}\|_{B^2}. \end{aligned}$$

The next part of the proof establishes consistency of both terms in the inequality above, i.e.

$$(i) \quad \left\| \left(\hat{C}_{B^2, H}^{1/2} (\hat{C}_{B^2, H} \oplus \alpha \hat{W}(k))^{-1} \ominus C_{B^2, X}^{1/2} (C_{B^2, X} \oplus \alpha W(k))^{-1} \right) X \right\|_{B^2} \rightarrow_{\text{a.s.}} 0,$$

$$(ii) \quad \|\hat{C}_{B^2, H}^{1/2} (\hat{C}_{B^2, H} \oplus \alpha \hat{W}(k))^{-1} \hat{\mu}_{B^2, H}\|_{B^2} \rightarrow_{\text{a.s.}} 0.$$

By focusing on term (i) and introducing the operator norm in the Bayes space $\|\cdot\|_{\text{op}, B^2}$ we can deduce

$$\begin{aligned} &\left\| \left(\hat{C}_{B^2, X}^{1/2} (\hat{C}_{B^2, X} \oplus \alpha \hat{W}(k))^{-1} \ominus C_{B^2, X}^{1/2} (C_{B^2, X} \oplus \alpha W(k))^{-1} \right) X \right\|_{B^2} \\ &\leq \left\| \left(\hat{C}_{B^2, X}^{1/2} (\hat{C}_{B^2, X} \oplus \alpha \hat{W}(k))^{-1} \ominus C_{B^2, X}^{1/2} (C_{B^2, X} \oplus \alpha W(k))^{-1} \right) \right\|_{\text{op}, B^2} \|X\|_{B^2}. \end{aligned}$$

Here, for the operator norm above observe that

$$\begin{aligned}
& \left\| \left(\hat{C}_{B^2, X}^{1/2} (\hat{C}_{B^2, X} \oplus \alpha \hat{W}(k))^{-1} \ominus C_{B^2, X}^{1/2} (C_{B^2, X} \oplus \alpha W(k))^{-1} \right) \right\|_{\text{op}, B^2} \\
&= \left\| \left(\hat{C}_{B^2, X}^{1/2} (\hat{C}_{B^2, X} \oplus \alpha \hat{W}(k))^{-1} \ominus \hat{C}_{B^2, X}^{1/2} (C_{B^2, X} \oplus \alpha W(k))^{-1} \right) \right. \\
&\quad \left. \oplus \left(\hat{C}_{B^2, X}^{1/2} (C_{B^2, X} \oplus \alpha W(k))^{-1} \ominus C_{B^2, X}^{1/2} (C_{B^2, X} \oplus \alpha W(k))^{-1} \right) \right\|_{\text{op}, B^2} \\
&\leq \left\| \hat{C}_{B^2, X}^{1/2} \right\|_{\text{op}, B^2} \left\| (\hat{C}_{B^2, X} \oplus \alpha \hat{W}(k))^{-1} \ominus (C_{B^2, X} \oplus \alpha W(k))^{-1} \right\|_{\text{op}, B^2} \\
&\quad + \left\| \hat{C}_{B^2, X}^{1/2} \ominus C_{B^2, X}^{1/2} \right\|_{\text{op}, B^2} \left\| (C_{B^2, X} \oplus \alpha W(k))^{-1} \right\|_{\text{op}, B^2}
\end{aligned}$$

First, since $\hat{C}_{B^2, X} \rightarrow_{\text{a.s.}} C_{B^2, X}$, there exists a bound on the operator norm of $\hat{C}_{B^2, X}$. Then, we have that

$$\begin{aligned}
\left\| (\hat{C}_{B^2, X} \oplus \alpha \hat{W}(k)) \ominus (C_{B^2, X} \oplus \alpha W(k)) \right\|_{\text{op}, B^2} &= \left\| \left(\hat{C}_{B^2, X} \ominus C_{B^2, X} \right) \oplus \alpha \left(\hat{W}(k) \ominus W(k) \right) \right\|_{\text{op}, B^2} \\
&\leq \left\| \hat{C}_{B^2, X} \ominus C_{B^2, X} \right\|_{\text{op}, B^2} + \alpha \left\| \hat{W}(k) \ominus W(k) \right\|_{\text{op}, B^2}.
\end{aligned}$$

As the projector onto the finite-dimensional subspace spanned by the first k -principal functions is a strongly consistent estimator, provided that $\lambda_k > \lambda_{k+1}$ (see e.g. Hall and Hosseini-Nasab (2006)), $\hat{W}(k)$ is also strongly consistent for $W(k)$. Therefore $\hat{C}_{B^2, X} \oplus \alpha \hat{W}(k) \rightarrow_{\text{a.s.}} C_{B^2, X} \oplus \alpha W(k)$. Furthermore, we have $\sup_n \left\| (\hat{C}_{B^2, X} \oplus \alpha \hat{W}(k))^{-1} \right\|_{\text{op}, B^2} \leq \alpha^{-1}$. This fulfills the assumptions of Lemma 8 in Berrendero et al. (2020) and we get $\left\| (\hat{C}_{B^2, X} \oplus \alpha \hat{W}(k))^{-1} \ominus (C_{B^2, X} \oplus \alpha W(k))^{-1} \right\|_{\text{op}, B^2} \rightarrow_{\text{a.s.}} 0$. Following these derivations we have

$$\left\| \hat{C}_{B^2, X}^{1/2} \right\|_{\text{op}, B^2} \left\| (\hat{C}_{B^2, X} \oplus \alpha \hat{W}(k))^{-1} \ominus (C_{B^2, X} \oplus \alpha W(k))^{-1} \right\|_{\text{op}, B^2} \rightarrow_{\text{a.s.}} 0. \quad (8)$$

Second, because of the consistency of $\hat{C}_{B^2, X}^{1/2}$ and the continuity of the square root we also have $\left\| \hat{C}_{B^2, X}^{1/2} \ominus C_{B^2, X}^{1/2} \right\|_{\text{op}, B^2} \rightarrow_{\text{a.s.}} 0$. Since for every $Y \in \mathcal{B}^2(I) : \left\| (C_{B^2, X} \oplus \alpha W(k))^{-1} \right\| \leq \alpha^{-1}$,

$$\left\| \hat{C}_{B^2, X}^{1/2} \ominus C_{B^2, X}^{1/2} \right\|_{\text{op}, B^2} \left\| (C_{B^2, X} \oplus \alpha W(k))^{-1} \right\|_{\text{op}, B^2} \rightarrow_{\text{a.s.}} 0. \quad (9)$$

Finally, (8) and (9) proof claim (i). For claim (ii) we can establish

$$\left\| \hat{C}_{B^2, X}^{1/2} (\hat{C}_{B^2, X} \oplus \alpha \hat{W}(k))^{-1} \hat{\mu}_{B^2, X} \right\|_{B^2} \leq \left\| \hat{C}_{B^2, X}^{1/2} \right\|_{\text{op}, B^2} \left\| (\hat{C}_{B^2, X} \oplus \alpha \hat{W}(k))^{-1} \right\|_{\text{op}, B^2} \left\| \hat{\mu}_{B^2, X} \right\|_{B^2}.$$

In a similar fashion as before we can determine that both operator norms above are bounded. Because of the assumption of this corollary we further have $\left\| \hat{\mu}_{B^2, X} \right\|_{B^2} \rightarrow_{\text{a.s.}} 0$ which concludes to

$$\left\| \hat{C}_{B^2, X}^{1/2} (\hat{C}_{B^2, X} \oplus \alpha \hat{W}(k))^{-1} \hat{\mu}_{B^2, X} \right\|_{B^2} \rightarrow_{\text{a.s.}} 0.$$

The proofs of (i) and (ii) now show that the initial claim $\left\| X_{\text{st}, \hat{C}_{B^2, X}}^{\alpha, k} \right\|_{B^2} \rightarrow_{\text{a.s.}} \left\| X_{\text{st}, C_{B^2, X}}^{\alpha, k} \right\|_{B^2}$ holds. The remaining proof of this corollary now directly follows from Proposition (3.4).

References

- Berrendero, J. R., B. Bueno-Larraz, and A. Cuevas (2020). On Mahalanobis distance in functional settings. *Journal of Machine Learning Research* 21(9), 1–33.
- Hall, P. and M. Hosseini-Nasab (2006). On properties of functional principal components analysis. *Journal of the Royal Statistical Society Series B: Statistical Methodology* 68(1), 109–126.
- Hildebrandt, T. H. (1912). Necessary and sufficient conditions for the interchange of limit and summation in the case of sequences of infinite series of a certain type. *Annals of Mathematics* 14(1/4), 81–83.
- Kokoszka, P. and M. Reimherr (2017). *Introduction to Functional Data Analysis*. Chapman & Hall / CRC numerical analysis and scientific computing. CRC Press.